5 Determination of Reliable Material Properties

E. Roos
Energie-Versorgung Schwaben AG (EVS)
Stuttgart, Germany

J. Föhl
Staatliche Materialprüfungsanstalt (MPA)
Universität Stuttgart, Germany

1 Introduction

The pressure retaining boundary of the primary circuit is subjected to complex loadings resulting from normal operation and exceptionally, from emergency conditions. To assure sufficient safety margins assuming that the structure contains flaws reliable material properties must be available. The safety margin can then be determined quantitatively when these parameters are considered in conjunction with the calculated stresses, strains and stress intensity values.

For the assessment of the safety margin, the ASME boiler and pressure vessel Code in the US and the KTA rules in Germany present normalized lower bound fracture toughness values for brittle crack initiation (static and dynamic) and crack arrest of commonly used reactor pressure vessel materials. In addition, methods are given which show how component specific lower bound fracture toughness curves can be derived from the normalized curves. These are based on material acceptance test data and surveillance results with respect to the design life time (DLT). The fracture mechanics requirements of these Codes, however, are limited to the linear elastic fracture mechanics regime and do not cover the elastic-plastic fracture mechanics regime. For all considerations the Charpy impact test and the data derived therefrom play a central role although this data do not directly allow the quantification of

the safety margin. Therefore, experiments with a variety of reactor pressure vessel steels of different quality, including irradiated materials, have been performed to prove the reliability of the implementation of the Charpy impact test into a quantitative fracture mechanics concept.

Additional consideration has been given in applying those results with particular regard to the size and geometry of the specimens and their transferability to complex structures. This considerations required a detailed understanding of the parameters affecting material failure as well as the development of experimental and analytical methods to describe the loading situation resulting from transients.

Much experimential effort has been undertaken to demonstrate the transferability of those results to the component in service by investigations on large scale specimens and model vessels.

While the changes in material as a Function of time is described in other chapters, the following part deals only with the applicability and transferability of results of given materials. It focuses on research work and on the validation of the underlying principles of the Code with regard to lower bound fracture toughness properties and analytical methods.

2 Evaluation of Fracture Mechanics Properties

Fracture mechanics data are needed for the whole temperature range of the operational loading regime. Because of the transition in fracture behaviour from brittle to ductile fracture, different theories in the linear elastic (LEFM) and the elastic-plastic (EPFM) regime have been developed and reliable fracture mechanics parameters must therefore be determined in both regimes. The lower bound fracture toughness curves of the Code are only valid for the LEFM regime.

2.1 Assessment of Reliable Fracture Mechanics Properties (LEFM)

The linear elastic fracture mechanics parameter is the fracture toughness (K_{Ic}). It characterizes the onset of brittle fracture and can therefore be regarded as a crack initiation value. The experimental determination of K_{Ic} values is described e.g. in the American Test Standard ASTM E 399 [1], and the British Standard BS 5447 [2]. Both standards are similar. The results are only valid in the range that satisfies the requirements of linear elastic (plain strain) conditions. In principle, those data should be size independent and their transferability to the real component should be expected. Tests were performed with either compact tension (CT) specimens or three point bend (TPB) specimens. For both types of specimens all other dimensions are related to the specimen thickness which is the most important parameter with respect to the constraints necessary to provide plain strain conditions. From experience a validity criterion has been defined with regard to the thickness requirement of the specimens

$$B \geq \omega \, (K_{Ic}/\sigma_y)^2$$

B	specimen thickness
K_{Ic}	fracture toughness value
σ_y	yield strength
ω	the validity criterion (material dependent)

According to the standards, ω is required to be ≥ 2.5, however, this value is still being considered because only limited information from large specimen testing is available. Data from testing large specimens indicated that even in the range where the validity criterion was fulfilled a further decrease in K_{Ic} values occurs with increasing specimen thickness as shown in Fig. 1. According to these test results lower bound values for K_{Ic} are yet reached at relatively high values of ω. This general problem is under international

discussion and is being reflected in the work of the appropriate ASTM Committee which has suggested using a value of $\omega \geq 4$ [3].

The fracture toughness of a material depends strongly on the temperature. A lower bound fracture toughness curve K_{Ic} as a function of temperature relative to the Reference Nil Ductility Transition Temperature RT_{NDT} is given in Fig. 2 for a high strength fine grained reactor pressure vessel (RPV) steel [4, 5, 6]. As a consequence of this behavior tests can be performed with small specimens at low temperature whereas large specimens are needed at elevated temperature.

2.2 Assessment of Fracture Mechanics Characteristics Based on Charpy-V Notch Impact and Drop Weight Tests

The reference fracture toughness curves as discussed in section 2.1 above and used in the fracture mechanics approach is adjusted onto an absolute temperature scale by using the Reference Nil Ductility Transition Temperature RT_{NDT}. This Reference Temperature is obtained from the Charpy-V notch impact test and the drop weight test [7], as discussed in Chapter 2. The determination of RT_{NDT} and thus the adjustment of the lower bound fracture toughness curve K_{IR} includes data scatter deriving from both the Charpy and the drop weight test.

Because of the significance of those data in the safety analysis, results obtained with two different reactor pressure vessel steels (22 NiMoCr 37 with 90 J upper shelf energy and 20 MnMoNi 55 with 200 J upper shelf energy), tested in 10 different laboratories in Germany were compared [8]. Eighteen specimens were machined and tested in a temperature range of -100°C to 350°C by each participant. The mean values of the energy for the high upper shelf energy material (KS 13) are plotted against the temperature in Fig. 3. The upper part of the figure shows the standard deviation assuming a Gaussian

normal distribution. The corresponding data for the lateral expansion also necessary to determine the RT_{NDT} is presented in Fig. 4. The test results include scatter deriving form the test machine and from the material. Similar behaviour was observed in the material with a low upper shelf valve of 90 J.

Since the data for the determination of the Reference Nil Ductility Transition Temperature RT_{NDT} are taken as the lower bound of three specimens tested at each temperature or from the lowest envelope of the energy-temperature curve, this procedure covers part of the scatter in a conservative way.

Ten laboratories participated in the drop-weight round robin test also each participant prepared its own specimens. The test results are shown in Fig. 5. The overall span of values was 30 K with a mean value at -25°C assuming a normal distribution. One of the main sources for the scatter was the individual evaluation of the sensitive criterion "break" or "no break" of the specimens. Discrepancies were observed between the evaluations of the fracture surface of the specimens and from the appearence of completely fractured specimens after heat tinting, especially in cases when the crack ran very closely to the edges. A more precise definition of the evaluation technique in Standards is desirable.

2.3 Elastic Plastic Fracture Mechanics Properties

Apart from the crack tip opening displacement (CTOD), the J-integral can be used to determine fracture mechanics parameters in the range of elastic-plastic material behaviour.

From the crack resistance curve (J_R-curve)

$$J = f(\Delta a)$$

J J-integral
Δa stable crack growth

characteristic values can be determined from individual points on the J_R curve. In the past, different procedures were developed to assess fracture toughness data.

J_{Ic}	according to ASTM E 813-88 [9]
J_i, $J_{0.2}$, $J_{0.2/bl}$	EGF P 1-90 [10]
J_i	JSME S 001-1981 [11]

The various criteria are defined in the corresponding standards. They make use of different algorithms to evaluate the J-integral from the load-line elongation results measured on the specimen and for the approximation of the J_R curve from J/Δa data pairs describing the crack resistance curve from which reliable crack initiation data are derived. An additional method has been introduced as a supplement to the existing standards to determine crack initiation values which are considered to be intrinsic material properties (physical initiation values) and thus can be transferred to complex components.

The characteristic data evaluated according to different methods are compared in Fig. 6. It is obvious that the data which are used to describe crack initiation differ quite markedly. In the example given the values vary from 85 N/mm to 167 N/mm.

With respect to transferability, it can be demonstrated that the physical crack initiation value J_i [12] is a reliable property to use. The evaluation is based on a special fit of the J/Δa data pairs and the intersection with an

experimentally determined blunting line derived from the "stretched zone" Δa_i. This is the region of extensive plastic deformation (crack tip blunting) developed before the onset of stable crack growth. The basic principle of this evaluation method is as follows: the stretched zone is completely formed during the blunting process and represents a "steady state volume" of highly deformed material which is maintained during the process of stable crack extension. Tests with different amounts of stable crack growth confirm the assumption of a constancy in the size of the stretched zone. After completion of the test, the stretched zone Δa_i can be measured on the fracture surface e.g. by means of the scanning electron microscope (SEM) and can be separated from stable crack growth Δa according to its different appearance. J_i is derived from the J_R curve as the intersection of the vertical line at Δa_i with the J_R curve, resulting in

$$J\ (\Delta a_i) = J_i$$

The J value obtained from this equation is called crack initiation parameter J_i, Fig. 7. For a reliable determination of the J_i value it is important that the difference between the approximation function and the $J/\Delta a$ points is minimized especially in the region of small crack growth. These features are neglected in the standards.

Nevertheless this procedure is comparable with the Japanese standard [11] and also with EGF P 1-90 [10]. The major difference can on the one hand be referred to the selection of the $J/\Delta a$ data points used to determine the crack resistance curve and on the other hand to the kind of polynomial approximation of the J_R curve.

For a comparison with K_{Ic} data obtained in the linear elastic regime, J values can be converted into K_I values according to

$$K_{IJ} = \frac{E \cdot J_i}{1-\nu^2}$$

E Young's modulus

ν Transverse contraction coefficient

K_{IJ} indicates that data was derived from J-integral test procedure

The J_i evaluation method is not only applicable in the plastic regime as, it is the Charpy upper shelf region, but also in the transition temperature regime. Scatter of data has, however to be taken into account.

When applying the different evaluation methods as seen in Fig. 6, sufficient safety margin against fracture is observed regardless of the evaluation method used - because of the large amount of crack growth before the occurrence of the fracture. The quantification of this margin in a real component is the aim of such a fracture mechanics analysis, additionally focusing on those parameters which give the best agreement with the failure behaviour of large and complex loaded structures.

The first step in investigating the transferability of fracture mechanics properties is a detailed analysis of the deformation behaviour of the individual laboratory specimen. To visualize the equivalence of the different crack initiation values, the data points are marked in different diagrams, Fig. 8, which are

a) load / crack opening displacement (COD)
b) load / stable crack extension (Δa)
c) J-Integral / COD, and
d) J-Integral / Δa

as obtained on a typical RPV steel 20 MnMoNi 55 with a 20% side grooved CT specimen (CT-25 mm) tested in the upper shelf

Charpy regime at 80°C. The position in the load / COD diagram indicates the margin from first crack initiation to maximum load carrying capability. This comparison shows clearly that the J_i value lies on the curve before maximum load while the "pseudo" properties ($J_{0.2}$, $J_{0.2/bl}$, J_{Ic}), related to crack initiation, fall together with maximum load or even in the dropping branch of the load curve after maximum load has been reached in the case of the J_{Ic} value being determined according to ASTM E 813-88.

With respect to the necessary safety margin in the design of a component, material characteristics which are strongly influenced by the testing and evaluation procedure cannot be accepted. Therefore of all J values, only the J_i value, which can be considered to be an intrinsic material property describing the physical crack initiation should be applied. Similarly, δ_i, the CTOD at initiation, yields a critical material property under given conditions, like temperature and loading rate.

2.4 Determination of Dynamic Fracture Mechanics Parameters

The lower limit fracture toughness curve (K_{Ia} or K_{IR}) specified in the Codes [4, 5, 6, 13] is based on crack arrest toughness (K_{Ia}) and on dynamic fracture toughness values (K_{Id}). However the loading rate at which the dynamic fracture toughness data should be determined has not been defined. Tests can either be performed with CT-specimens in servo-hydraulic machines and rotary disc impact machines or with 3 point-bend specimens in pendulum and drop weight impact machines. Typical load rates are applied up to $\dot{K} = 10^6$ MPa$\sqrt{m}$/s. Only few test standards exist for the determination of dynamic fracture mechanics parameters. As a first step towards the standardization, ASTM have specified loading rates of $\dot{K} > 2.75$ MPa$\sqrt{m}$/s [1] in the linear elastic

regime. Similar loading rates, ranging from $2.5 < \dot{K} < 3200$ MPa$\sqrt{m}$/s, are required in the British Standard [14]. According to those Standards tests can also be performed at higher loading rates if reliable techniques are available to measure load and load-line displacement during the dynamic test. This derives from tests on CT-specimens [15]. In the elastic plastic regime the requirements are similar to those specified in ASTM E 813 [9], but extended to a higher loading rate. Inertial forces are not considered in this evaluation of the J-integral which is equivalent to quasi-static loading conditions.

In recent studies, dynamic tests were performed at impact velocities from 0.04 to 20 m/s corresponding to loading rates in terms of $\dot{K}_I$ of 1 to 1.5 · 10^6 MPa$\sqrt{m}$/s [16] with CT-specimens of 15 mm thickness containing 20% side grooves. The validity of the test results was evaluated on the basis of the existing standards [1, 9, 14] using the dynamic yield strength of the material determined with smooth round tensile bars under equivalent strain rate as calculated for the edge of the plastic zone in the CT specimens.

In Fig. 9 dynamic fracture toughness data of a RPV material 20 MnMoNi 55 (KS 17) with high upper shelf toughness (USE = 200 J) are compared with data obtained from quasi static testing. All tests were performed using CT specimens. The dynamic fracture toughness data are at the lower end of the quasi-static values or even lower. The fracture toughness decreases further with increasing load rate which has the global effect of a shift in fracture toughness to higher temperature. In the linear elastic regime, the dynamic testing yields higher fracture toughness data compared with the K_{Ia}-curve. This provides validation of the K_{Ia} curve as a lower bound in this regime.

2.5 Evaluation of Crack Arrest Parameters

The crack arrest toughness is the plain strain elastic stress intensity at the arrest point. It can be determined by means of modified compact specimens, wide plates and rotating discs. The use of transversely wedge loaded compact specimens has proven to be the simpliest and most favoured method, Fig. 10. The crack in the specimen is usually initiated in a brittle weld introduced at the location of the notch. In high strength material the notch can be produced directly by means of electric discharge machining (EDM) of the specimens, which simplifies considerably the specimen preparation. The test requirement and the evaluation the K_{Ia} value is decribed in ASTM E 1221-88 [17]. The crack arrest toughness is calculated on the basis of the crack tip opening displacement and the crack length at arrest for the given specimen dimensions. However, the K_{Ia} values are only valid if plain strain conditions and linear elastic material behaviour during the phase of crack extension is assured.

In Fig. 11, results of static (K_{Ic}) and dynamic (K_{Id}) fracture toughness values are compared with crack arrest toughness (K_{Ia}) and Charpy-V-notch energy as a function of temperature for the high toughness material 20 MnMoNi 55. According to the validity criteria the fracture toughness values do not encompass the temperature range of the entire Charpy curve but only that up to the transition temperature regime. In the lower shelf regime of Charpy energy the K_{Id} values lie invariably below the K_{Ic} and K_{IJ} values, respectively. The K_{Ia} values are in the main below the scatter band of each K_{Ic}, K_{IJ} and K_{Id}. Due to the wide scatter of the results, a definite correlation has not be established between the different toughness values.

A summary of the results discussed above is shown in Fig. 12. Where the lower limit curves of the K_{Ic} or K_{IJ} scatter bands taken from figure 11 and additionally tested materials, together with the K_{IR} reference curve, the lower limit for K_{Id} and K_{Ia} values and the K_{Ic} curve as the lower limit for initiation values are related to the Nil Ductility Transition Temperature T_{NDT}. This representation clearly demonstrates that within the validity range of linear-elastic fracture mechanics the lower limit curves of all materials fall above the K_{Ic} curve. Thus the K_{Ic} curve can be used as a conservative approximation. In the upper transition range and on the upper shelf, only the K_{IJ} values of 15 MnNi 6 3 exceed the limit of 220 MPa $\sqrt{m}$ specified in the Codes [5, 6, 13].

For the "other materials" it can, therefore, be concluded that for the upper shelf the K_{Ic} curve provides a non-conservative estimation of the actual fracture toughness derived from the initiation value.

A comparison of K_{Id} and K_{Ia} values with the K_{IR} reference curve is shown in Fig. 13. All values, except those of the low upper shelf energy of 40 J material 22 NiMoCr 3 7 (modified), manufactured for research purpose only, exceed the K_{IR} curve. This confirms the description of the K_{IR} curve as the lower envelope of the fracture toughness values (static and dynamic) - at least on the lower shelf and in the transition regime of the C_v-T curve.

Contrarily the lower limit curve of the K_{Ia} band of the low shelf material 22 NiMoCr 3 7 (modified) increases slightly with rising temperature and intersects the K_{IR} curve at approx. 40 K above T_{NDT} (= 70°C). This makes the conservative nature of the reference curve doubtful. Similar results are available for a second high-strength, low-toughness model material [18]. The results do not allow conclusion to be drawn about crack arrest behaviour on the upper shelf.

3 Transferability of Fracture Mechanics Properties from Small Scale Specimens to Components

The standard test conditions and evaluation procedures (compare with section 2 above) provide fracture toughness data which is transferable to any structure - regardless of size and dimensions - as long as the validity criteria are fulfilled. This has been proven in the linear elastic fracture mechanics regime for K_{Ic} [16], with the exception of the validity limitation depending on the size criteria for plain strain conditions (compare 2.1 and 3.2 above).

For the elastic-plastic fracture mechanics regime it has to be demonstrated that the physical initiation process does indeed begin at the level of J_i which was found to be size independent in case of CT specimens. Also a correlation has to be established between crack resistance, as given by the J_R curve, and the specimen geometry and size.

3.1 Evaluation of Fracture Mechanics Characteristics on Large Scale Specimens

A large worldwide effort has been undertaken in order to develop transferabilty criteria in the elastic-plastic fracture mechanics regime. One of those projects was the research program "Integrity of Components" in Germany [19]. Tests were carried out with large scale specimens made of fine grained structural steel of different quality covering high and extremely low Charpy upper shelf toughness. The crack initiation values and the crack resistance curves were compared with those from small scale specimens. The variety of specimens tested is shown in Fig. 14, it comprises CT specimens with a thickness up to 200 mm, single edge cracked tensile (SECT) specimens, double edge cracked tensile (DECT) specimens, centre cracked tensile (CCT) and three point bend (TPB) specimens with a width (B) ranging from 100 to

600 mm and a thickness (W) of up to 200 mm. The J_R curves experimentally determined with different large scale specimens are shown in Fig. 15a and b in comparison with the J_R curves evaluated from CT-specimens. The specimens in Fig. 15a were made of a fine grained structural steel 22 NiMoCr 3 7 (KS 01) with an upper shelf energy of about 90 J, the specimens in Fig. 15b were made of the modified low toughness material 22 NiMoCr 3 7 (KS 07) with a Charpy upper shelf energy of 40 J. The same crack initiation value J_i could be evaluated on all specimens as defined in section 2.3 above (converted to K_{IJ}) within a reasonable scatter band as usual for this type of test. Moreover the data corresponded with that derived from small scale specimens (CT-25 mm, 20% side grooved). This clearly demonstrates J_i to be a material property, not depending on size and geometry and thus a basis for application to large and complex structures and components. A biaxial stress state exists on traction free surfaces as it is at the crack tip. In case of compressive stresses resulting e.g. from internal pressure, yielding at the crack tip is promoted by the triaxial stress state - with one compressive principal stress component.

With regard to crack resistance (process of stable crack growth), however, there is a strong size and geometry effect [20] which, additionally, seems to depend on the material toughness. Tests performed at the onset of upper shelf show consistence in crack initiation J_i but not in the course of the crack resistance curve. This is due to the distinct differences in the degree of multiaxiality of the stress state as they are associated with the selected specimen geometries and sizes. The degree of multiaxialty can be quantified by the equation

$$q = \frac{1}{\sqrt{3}} \frac{\sigma_e}{\sigma_m}$$

q degree of multiaxiality [21]
σ_e equivalent stress according to von Mieses
σ_m mean stress 1/3 $(\sigma_1+\sigma_2+\sigma_3)$

The lower the value of q, the higher the degree of multiaxiality. For the hydrostatic stress state (where q = 0) no plastic deformation (except void formation) can occur even in high toughness material.

The degree of multiaxiality is not constant across the specimen ligament and depends on the relative crack length (a/W) as shown for a DENT specimen in Fig. 16. In case of a modest crack length (a/W = 0.5), q is a minimum in front of the crack tip and increases across the ligament. For deeply cracked structures (a/W = 0.8) q remains nearly constant across the ligament at a relatively low level - which indicates a high degree of multiaxiality.

The strong influence of geometric parameters on crack resistance can also be evaluated from tests performed on pipes in Japan [22] and on CCT specimens in the USA [23]. The pipe tests (circumferential slit, a/W = 1) were carried out under additional bending loads with systems of different stiffness. Although detailed fracture mechanics analyses are not yet available, the test results demonstrate the general influence of the geometry on the crack resistance curve J_R, Fig. 17. Under extreme conditions spontaneous fracture can occur in the component without any detectable stable crack growth as in the case of double edge notched tensile specimens with a crack length ratio of a/W = 0.8, Fig. 18.

The influence of material toughness on both the absolute value and the variation of q across the ligament can be demonstrated on materials with different Charpy upper shelf energy. After a certain amount of plastic deformation material separation occurs initially in the area where q reaches the critical value. In structures with q values close to critical value q_c

in a large part of the ligament, stable crack growth cannot be expected. This was the case for the DENT specimen (compare Fig. 18) where unstable crack growth (spontaneous fracture) occurred at the crack initiation value J_i. Structures of high toughness material in terms of Charpy upper shelf energy can mitigate the multiaxiality of the stress field by a greater amount of plastic deformation or void formation. This results in higher q values and thus reduces the risk of unstable crack extension causing brittle failure.

The q-value indicates wether or not stable crack extension is possible at given temperature. However, it provides, at present, no basis to transform J_R curves of a CT specimen to other specimen geometries or structures.

3.2 Application of Fracture Mechanics Concepts for Thermal Shock Experiments

In case of loss of cooling accidents (LOCA) water is injected into the RPV at low temperature to cool the nuclear core. This leads to transient conditions causing high thermal stresses in addition to the stresses resulting from internal pressure (pressurized thermal shock, PTS). In order to describe the behaviour of the RPV under those conditions much experimental and theoretical research work has been carried out to validate the fracture mechanics concepts. The investigations not only focused on crack initiation and crack extension but also on crack arrest. They included wide plates with thermal gradients and superimposed axial load, nozzles in large vessels and hollow cylinders under internal pressure and thermal gradients.

Wide plate tests were performed with materials having a toughness gradient across the plate thickness to simulate the effect of neutron irradiation [24]. The wide plates contained surface fatigue cracks in the less tough material and were subjected to asymmetric thermal shock loading. The external

load was applied as axial tension or 3 point bending. The aim of the tests was to demonstrate that even in materials, the toughness of which corresponds to the state at the end of design life time (DLT), brittle crack extension did not occur under PTS loading conditions. The test conditions were typical of the cylindrical wall and the nozzle corner region in the upper shelf toughness and the ductile/brittle transition regime.

Investigations on different sized hollow cylinders were carried out Fig. 19. Within the Heavy Section Steel Technology Program (HSST) tests with regard to thermal shock loading were performed at the Oak Ridge National Laboratory (USA) already in 1973 [25].

The first series of tests were loaded by thermal stresses only without internal pressure (Thermal Shock Experiments, TSE 1-6). These conditions were achieved by submerging an open hollow cylinder into liquid nitrogen after it had been heated homögeneously up to 100°C. To build up sufficient thermal stresses the cylinders contained long axial flaws with one exception (TSE-2) which was prepared with a semi-elliptical flaw. All failures occured in the linear elastic fracture mechanics regime. Crack initiation and crack arrest was in accordance with the predictions derived from lower bound fracture toughness values of small scale specimens. The tests gave no indication that dynamic fracture processes played any role. On the basis of the lower bound fracture toughness curves, presented in the ASME Code, all test results could be describee in a conservative way, Fig. 20.

In the Federal Republic of Germany, thermal shock experiments were carried out with thick walled hollow cylinders (emergency cooling simulation programme NKS) at MPA Stuttgart and on a full size vessel at the HDR plant (decommissioned superheated steam reactor). The hollow cylinders were fabricated from different steel qualities with Charpy upper shelf energy

ranging from 200 J to 40 J. The low shelf material had a nil ductility transition temperature - evaluated from Charpy energy/temperature curve - of about 250°C. Internal pressure and external axial load was applied on the hollow cylinder (O.D. = 800 mm I.D. = 400 mm) while the inner surface was cooled down rapidly from 300°C to room temperature. The loading conditions during the transient for the test specimen which contained an inner surface circumferential crack could be described by means of the J-Integral - as shown in the left part of Fig. 21. After a cooling time of about 7 min, the maximum J-value of about 430 N/mm was reached in this experiment (NKS-3). The stress and deformation analysis was carried out axial-symmetrically taking non-linear material behaviour into account. Calculations have shown that the degree of multiaxiality in the test specimen was of the same order as the one in the CT specimen. Therefore the J_R curve of a corresponding temperature which is plotted in the right part of Fig. 21 can be used for stable crack growth assessment. On the fracture surface a stable crack extension of 3.6 mm could be measured, Fig. 22, which is in good agreement with the calculated value of 3.5 mm as shown in Fig. 20 and thus validates the fracture mechanics concept and the applied FE analysis [26].

In reality, the cooling of the vessel during LOCA is not symmetrical for the vessel but occurs locally being concentrated at the nozzle corner and the cylindrical wall in the form of strip-cooling. The phenomena associated with this loading condition was investigated at the HDR pressure vessel by introducing "guided" cooling. FE analyses have indicated a more severe situation for a circumferential crack than for an axial one. Therefore circumferential cracks were produced in the RPV wall by milling, with subsequent fatiguing by cyclic thermal shock loading. In addition, cracks were produced in the nozzle corner region by cyclic thermal shock and then subjected to rapid cooling under internal pressure (PTS). The maximum crack depth for both locations, cylindrical wall and

nozzle corner, was approximately 15 mm. Within the time range investigated the J-integral increased steadily with time for the cracks in the cylindrical wall, but dropped after having reached the maximum in a short time for the nozzle corner crack, Fig. 23. The principal differences in loading condition result from axi-symmetric cooling in the nozzle area and non-symmetric cooling in the cylindrical wall [27].

According to the J_i values represented by the scatter bands for different circumferential specimen orientations corresponding to the crack growth directions (T-S nozzle crack, L-S crack in cylinder) plotted in Fig. 23, crack initiation and a certain amount of stable crack growth should have occurred for the crack in the cylindrical wall. Fractographic investigations, however, have not given any indication of stable crack growth. Only in a few areas could signs of incipient stretched zones at the fatigue crack tip be identified. The discrepancy between prediction of stable crack growth by the calculation and the absence of crack extension in the test must be referred to the extensive crack branching and thus to a relief in stress intensity, Fig. 24 [27].

Comparable thermal shock experiments have been conducted at the European Joint Research Center (JRC) in Ispra, Italy on nozzle corner cracks [28]. In the United Kingdom thermal shock experiments were performed on thick walled hollow cylinders spinning at a high revolution rate with a longitudinal crack along the whole length of the inner surface [29].

From the results of the wide-plate experiments it can be concluded that the transferability of data is valid even for complex structures and loading conditions. The application of the crack resistance curve to other specimens and structures, is, however, only possible when the stress states are comparable.

3.3 Crack Arrest Behaviour

The main feature of crack arrest studies with CT-specimens, as described in section 2.5 above, is that the crack grows into a decreasing K-field. Arrest in an increasing K-field is only possible when the crack initiates in a low toughness material and extends towards a region of higher toughness. This situation corresponds to a neutron irradiated vessel, assuming a crack is initiated at the inner surface and penetrates towards the outside. The necessary toughness gradients can be obtained in the test specimen either through a temperature gradient across a specimen section or by the use of a composite specimen [24, 30]. Most commonly used are tests where the toughness gradient is generated by a stationary thermal gradient in a single edge cracked wide plate specimen and the loading is applied by axial tension. Crack arrest toughness values of different materials determined under different test conditons, e.g. thermal shock (TSE) and pressurized thermal shock experiments (PTSE) on vessels in USA [25] and in France (FTSE) [31], wide plate tests in Japan (ESSO) [24], in USA (WP-1, WP-2) and Germany (GP-1) were found to be all enveloped by the crack arrest curve from the Codes, Fig. 25.

High crack arrest toughness values of up to 400 MPa$\sqrt{m}$ result from the American wide plate tests (WP) and the Japanese ESSO tests. The crack arrest values derived from the thermal shock vessel experiments are generally lower than those from wide plates but they are still higher than the upper limit according to the Codes. The lowest crack arrest toughness values were obtained in the French thermal shock experiments (FTSE) which were carried out at a temperature of 20 K above RT_{NDT}. The results of the German wide plate experiments and the rotating disc experiment fall within the scatter band of all the other results [30]. Contrary to the other results, a kind of upper bound toughness tending towards 200 MPa$\sqrt{m}$ can be observed from the wide plate test GP 1 (see Fig. 25). The test

material KS 22 is a low toughness material (USE = 40 J) with high transition temperature (-250°C) which was produced for research purposes. Similar results on the same materials were also obtained from CT specimens, Fig. 26 [18].

At present, there is no ready explanation for the extremely high arrest values determined for some of the wide plate tests which are higher than the crack initiation values of materials with high upper shelf Charpy energy. Conclusions on the transferability of crack arrest results in the elastic-plastic regime cannot yet be drawn.

3.4 Summary of Transferability

To summarize the present state on fracture mechanics characteristics. Lower limit curves for K_{Ic} and K_{IJ} derived from J_i have been compared with the Code K_{Ic}, K_{Ia} and K_{IR} curves. Within the linear-elastic regime, the Code curves cover the experimental results for all the investigated materials in a conservative way. However, in the Charpy upper transition range and the upper shelf regime the experimentally determined data intersect the K_{Ic}, K_{Ia} and K_{IR} curves depending on the toughness of the material. It therefore has to be concluded, that the K_{Ic} curve is not conservative for all materials with respect to crack initiation on the upper shelf.

4 Correlation of Fracture Mechanics Properties with Charpy V-Notch Energy

In general fracture toughness data are not available for actual material of a reactor pressure vessel. From surveillance programmes, however, Charpy-V notch energy data are determined with the aim of using that data for a quantitative safety analysis based on fracture mechanics

considerations. To evaluate the effects of size and multiaxiality a correlation between Charpy transition regime and Nil Ductility Transition Temperature can be derived on an empirical basis. In the upper shelf regime to obtain a correlation between the dynamically absorbed energy to fracture and the quasi-statically evaluated J initiation value (J_i) is much more difficult.

Regardless of any physical solution, a correlation between Charpy energy and initiation fracture toughness has been established on an empirical basis. From statistical evaluation of 200 different melts of 22 different ferritic materials a tangent hyperbolic (tanh) fit was used to convert Charpy data into fracture toughness data covering the complete temperature range [32]. The evaluation of a A 508 Cl 2 steel shows good agreement with measured fracture toughness values up to the transition regime within a confidence limit of 95%, Fig. 27. Major differences occur in the upper shelf regime. More correlations between static and dynamic fracture toughness values and Charpy test results are summarized in Ref. [33].

From experimentally determined J_i values and the corresponding upper shelf Charpy energy (USE), a statistical correlation between J_i and USE has been established, Fig. 28 [34]. All experimental J_i data falls beyond the curve $J_i - 2\sigma$ with a probability of 97.73%. In addition another correlation is shown in this figure, which takes besides the Charpy energy the mean flow stress σ_{fl} and stable crack extension into account [35]. This curve is similar to the one mentioned above and falls between the two curves $J_i-\sigma$ and $J_i-2\sigma$. On the basis of this correlation a complete J_R curve can be derived in the elastic-plastic fracture mechanics regime from Charpy upper shelf energy. In the correlation the two discrete data for Δa = 0.1 and 0.2 mm were selected (see Fig. 25) because Δa = 0.1 mm matches quite well with the stretched zone of a highly tough material wheras Δa = 0.2 mm represents the region of the

technical material characteristics on the J_R curve according to ASTM E 813-88 and EGF P 1-90.

5 Summary

Since the transferability of the J_R curves is not allowed in general as described a comparison of calculated J_R curves with experimental data is not considered here.

The fracture mechanics limit curves given in the main Codes for initiation K_{Ic}, crack arrest K_{Ia} and the reference curve K_{IR}, covering crack arrest as well as dynamic fracture mechanics data, are conservative when compared with all test results, if linear elastic (plain strain) conditions can be assumed. In the transition regime, and on the upper shelf - depending on the material involved - these curves exceed the actual fracture toughness. Thus, predictions based on these curves can be non-conservative in these toughness regimes.

The effective crack initiation values J_i are independent of the size and geometry of the specimen or component at given temperatures and loading rates and, therefore, are material properties transferable to components. However, this does not apply to the crack resistance curves which strongly depend on the degree of mulitaxiality of the stress state. With increasing material toughness not only the effective crack initiation value J_i but also the tearing resistance against stable crack growth will increase as well. This holds also for complex loading conditions (pressurized thermal shock) and complex component shape (e.g. nozzle corner crack).

[1] ASTM E 399-88, Standard Test Method for Plane-Strain Fracture Toughness of Metallic Materials. Annual Book of ASTM Standards, Vol. 03.01.1988.

[2] BS 5447: Method of Plane Strain Fracture Toughness Testing. British Standards Institution, 1977.

[3] International Standard, ISO 7539-6, Corrosion of Metals and Alloys - Stress Corrosion Testing - Part 6: Preparation and Use of Pre-Cracked Specimens, 1989.

[4] ASME Boiler and Pressure Vessel Code, Section XI, Division 1, Appendix A, 1988

[5] KTA 3201.2, Fassung 3, 1984, Sicherheitstechnische Regeln des KTA; Komponenten des Primärkreises von Leichtwasserreaktoren Teil 2: Auslegung, Konstruktion und Berechnung.

[6] Règles de conception et de construction des Matériels Mécaniques des Nucléaires PWR. RCC-M, Annexe ZG, [Edition 1988],AFCEN (Associoation Francaise pour les Regles de Conception et de Construction des Materiels des Chaudieres Electro-Nucleares)

[7] ASME Boiler and Pressure Vessel Code Section III Div. 1 NB-2000 (Edition 1986)

[8] Langer, R. and Pröger, M., "Vergleichsversuche in verschiedenen Laboratorien (Round Robin Test) zur Beurteilung des Zähigkeitsverhaltens der Werkstoffe im Forschungsvorhaben Komponentensicherheit". 5th MPA-Seminar, Okt. 1979, Stuttgart, Germany. Schweissen Schneiden,ISSN 0036-7184,(July 1980)

[9] ASTM E 813-88, Standard Test Method for JIc, A measure of Fracture Toughness. Annual Book of ASTM Standards, Vol. 03.01.1988.

[10] EGF P1-90, European Group of Fracture)EGF) Recommendations for Determining the Fracture of Ductile Materials. December 1989

[11] JSME-Japan Society of Mechanical Engineers, Committee S 781/JSME Standard S 001-1981, 1991

[12] Roos, E. and Eisele, U., Determination of the Materials Characteristic Values in Elastic-Plastic Fracture Mechanics by Means of J-Integral Crack Resistance Curves, Journal of Testing and Evaluation, Vol. 16, No. 1, 1988, pp 1-11

[13] ASME Boiler and Pressure Vessel Code Section III, Division 1, Appendix G, 1988

[14] BS 6729, British Standartd Method for Determination of the Dynamic Fracture Toughness of Metallic Materials. British Standards Institution, 1987

[15] Kussmaul, K., Demmler, T. and Klenk, A., OptoElectronic Measuring Methods in Dynamic Elastic-Plastic Fracture Mechanics; 7th International Conference on Fracture, 20-24 March 1989, Houston, USA. Pergamon Press, 1989

[16] Shoemaker, A.K., Factors Influencing the Plane-Strain Crack Toughness of Structural Steels, ASME J. Bas. Eng. 9 (1969) pp. 506-11

[17] ASTM E 1221-88, Standard Test Method for Determining Plane-Strain Crack-Arrest Fracture Toughness, KIa of Feritic Steels Annual Book of ASTM Standards, Vol. 3.1.1988

[18] Kussmaul, K. and Gillot, R., Determination of Crack Arrest Toughness at High Temperatures Using Compact Specimens: Journ. Pressure Vessel Technology 110 (1988) pp. 129-36

[19] Kussmaul, K., Föhl, J. and Roos, E., Some Conclusions with Regard to the Safety Assessment of Cracked Components Drawn from the Research Program Integrity of Components (FKS II) at the Present State. Proceedings. 12th MPA Seminar, October 1986, Stuttgart, Germany. Nuclear Engineering Design, Vol. 102, July 1987

[20] Roos, E., Eisele, U., Silcher, H. and Spaeth, F., The Influence of the Material Toughness and the State of Stress on Fracture of Large Scale Specimens, Nuclear Engineering and Design, 102 (1987), pp. 429-49

[21] Clausmeyer, H., Kussmaul, K. and Roos, E., Influence of Stress State on the Failure Behaviour of Cracked Components Made of Steel, Appl. Mech. Rev. Vol. 44 (1991) No. 2, pp. 77-92

[22] Miyazono, S., Shibata, K. and Ueda, S., Fracture Behaviour of Circum,ferentially Cracked Pipes under Bending Load. 3rd German-Japanese Joint Seminar, 1985, Stuttgart, Germany
Nuclear Engineering and Design, July 1986, v.94(3), pp. 221-231

[23] Wilkowski, G.M. et al, Summary of NRC Phase I Degraded Piping Program. Instability Analyses and Review of Experimental Programs to Evaluate J/T Instability Predictions. ASME, J. Pressure Vessels and Piping, 95, (1985) pp. 223-254

[24] Yagawa, G., Ishihara, K., Ando, Y., Iwadate, T. and Tanaka, Y., Stable and Unstable Crack Growth of A 508 cl. 3 Plates Subjected of Combined Force of Thermal Shock and Tension. Proceedings of International Meeting on Thermal Nuclear Reactor Safety, Sept. 1982, Chicago,IL, USA NUREG/CP-0027,vol.1

[25] Whitmann, G.D., Historical Summary of the Heavy-Section Steel Technology Program and Some Related Activties in Light Water Reactor Pressure Vessel Safety Research. NUREG/CR 4489, ORNL-6259, 1986

[26] Roos, E. and Guth, W., Investigations Concerning the Crack Resistance Behavior of Thick-Walled Components Under Thermal Shock Loading. Steel Research 61, No. 4 (1990), pp. 188-193

[27] Kussmaul, K., Roos, E., Diem, H., Katzenmeier, G. and Neubrech, G.E., Fracture Mechanics Assessment of Crack in the HDR Reactor Pressure Vessel due to Pressurized Thermal Shock Loading
11th International Conference on Structural Mechanics in Reactor Technology (SMIRT), August 18-23, 1991, Tokyo, Japan Atomic Energy Society of Japan,1991, Vol.G, pp.141-152

[28] Jovanovic, A. and Lucia, A.C., Analysis of Crack Behavior in the IRC-Ispra Pressurized Thermal Shock Experiments.
Nuclear Engineering and Design, 119 (1990) pp. 263-279

[29] Lacey, D.J. and Leckenby, R.E., Determination of Upper Shelf Fracture Resistance in the Spinning Cylinder Test Facility. 10th International Conference on Structural Mechanics in Reactor Technology (SMiRT), 14-18 Aug. 1989, Anaheim, USA. American Association for Structural Mechanics in Reactor Technology, Los Angeles, CA, USA, vol. F, pp.1-6

[30] Roos, E. and Griesinger, H., Crack Arrest Investigations on Rotating Disks
Int. J. Pressure Vessel and Piping 30 (1987), pp.23-36

[31] Brust, F.W., The Use of New Path Independent Integrals in Elastic-Plastic and Creep Fracture
PHD-Thesis, Georgia Institute of Technology, Atlanta, USA, November 1984

[32] Bamford, W., Oldfield, W. and Marston, T., An Improved Reference Fracture Toughness Procedure for Pressure Vessel Steels.
5th Int. Conference on Pressure Vessel Technology, 9-14 Sept. 1984, San Francisco, USA, Vol. 2, pp. 932-965
CEA-CONF-7461

[33] Roberts, R. and Newton, C.,
Interpretative Report on Small-Scale Test Correlations with KIc data. Water Resources Centre (WRC)-Bulletin 265, USA

[34] Kussmaul, K. and Roos, E., Statistical Evaluation of Post-Yield Fracture Mechanics Properties on the Basis of Notched Bar Impact Test
Nuclear Eng. and Design 87 (1985), pp. 123-137

[35] Dougan, J.R., Relationships between Charpy-V-Notch Impact Energy and Fracture Toughness
NUREG/CR-2362, ORNL/TM-7921, 1982

Fig. 1: Experimentally determined K_{Ic} values evaluated according to ASTM 399 in comparison with different validity criteria for thickness

Fig. 2: Lower bound fracture toughness curves as a function of temperature relative to the "Nil Ductility Reference Temperature" RT_{NDT}

Fig. 3: Mean curve, standard deviation and mean deviation of Charpy-V notch test results performed in different laboratories

Fig. 4: Mean curve, standard deviation and mean deviation of lateral expansion from tests shown in Fig. 3

Fig. 5: Nil Ductility Transition Temperature (NDT) determined from drop-weight tests in different laboratories

Fig. 6: Evaluation of stable crack initiation values according to different standards and methods; material 20 MnMoNi 5 5, USE = 200 J

Fig. 7: Method to determine crack initiation parameter J_i

Fig. 8: Comparsion of different crack initiation values on the load traces

a) load / COD, b) load / Δa,
c) J / COD, d) J / Δa

Fig. 9: Comparison of fracture toughness data obtained from quasi-static and dynamic tests

Fig. 10: Schematic view of a wedge loaded CT specimen to determine crack arrest toughness data

Fig. 11: Static and dynamic fracture toughness (K_{Ic}, K_{IJ}, K_{Id}), crack arrest toughness (K_{Ia}) and Charpy-V notch energy (C_v) as a function of temperature for RPV Steel 20 MnMoNi 5 5 (KS 17)

Fig. 12: Lower bound fracture toughess curves of different materials relative to NDT-temperature in comparison with the corresponding reference curves (K_{Ic} and K_{IR})

Fig. 13: Dynamic fracture toughness (K_{Id}) crack arrest toughness (K_{Ia}) relative to NDT-temperature for different materials

Fig. 14: Fracture mechanics specimens tested for investigation of transferability criteria

Fig. 15a: J_R curves of large scale specimens of different size and geometry; material 22 NiMoCr 3 7 (USE 90 J), specimen dimensions

DECT	B = 300,	W = 100
SECT	B = 300,	W = 200

Fig. 15b: J_R curves of large scale specimens of different size and geometry; material 22 NiMoCr 3 7 (modified, USE 40 J),

CCT	B = 200,	W = 300
TPB	B = 500,	W = 200
SECT	B = 300,	W = 200
DECT	B = 250,	W = 70

Fig. 16: Change of multiaxiality q across the ligament of double edge notched tensile (DENT) specimens with different crack length a/W

Fig. 17: J_R curves determined in pipe tests with different crack geometries and stiffness of the test set up

Fig. 18: J_R curves of low upper shelf double edge notched tension (DENT) specimens with different crack length

Fig. 19: Test specimen, model vessel and full size vessel used for pressurized thermal shock (PTS) experiments

Fig. 20: Fracture toughness values derived from thermal shock experiments in comparison with the ASME K_{Ic} and K_{Ia} curve

Fig. 21: Calculated J values (left hand side) during pressurized thermal shock (NKS-3) experiment in comparison with a J_R curve determined with a CT 10 specimen (right hand side) to derive amount of stable crack growth during experiment

Fig. 22: Crack depth in PTS specimen NKS-3 before and after test and average stable crack extension derived

Fig. 23: Calculated J-values as a function of time during the HDR thermal shock experiment

Fig. 24: Crack configuration in the cylindrical wall of the HDR vessel

Fig. 25: Crack arrest toughness data determined with large scale specimens in comparison with the ASME K_{Ia} curve

Fig. 26: Crack arrest toughness data as a function of temperature for materials with different upper shelf energy in comparison with the ASME Reference Curve (K_{IR}) (20 MnMoNi 5 5 USE = 200 J; 22 NiMoCr 3 7 modified USE = 40 J; 17 MoV 8 4, USE = 40 J)

Fig. 27: Fracture toughness data converted from Charpy-V notch energy in comparison with experimental K_{Ic} data of a A 508 Cl 2 steel

Fig. 28: Correlation of crack initiation values (J_i) with Charpy upper shelf energy

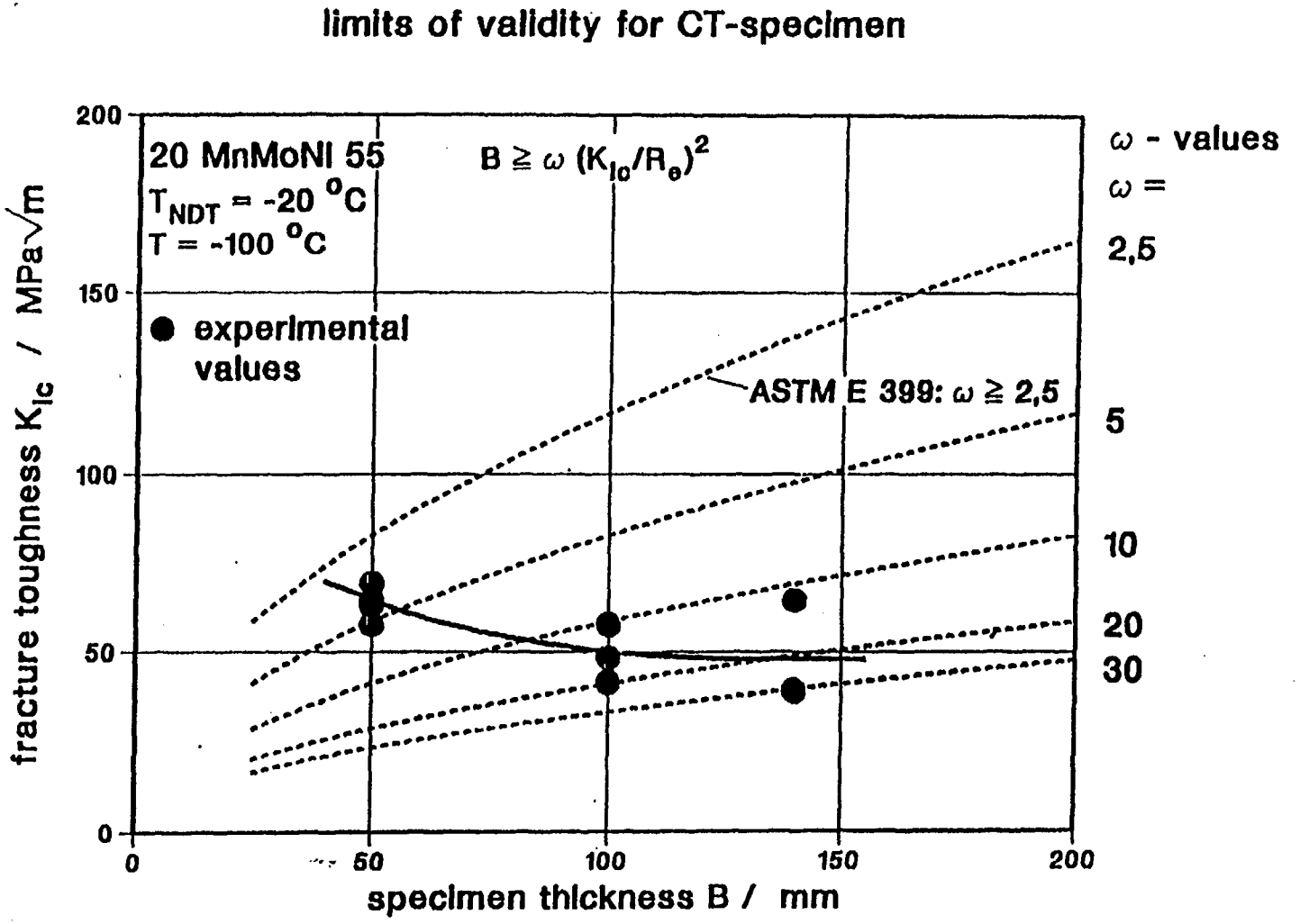
limits of validity for CT-specimen
20 MnMoNI 55
T_{NDT} = -20 °C
T = -100 °C
$B \geq \omega (K_{Ic}/R_e)^2$
experimental values
ASTM E 399: $\omega \geq 2,5$
ω - values
ω =
2,5
5
10
20
30
fracture toughness K_{Ic} / MPa√m
specimen thickness B / mm
0
50
100
150
200

FIGURE 1

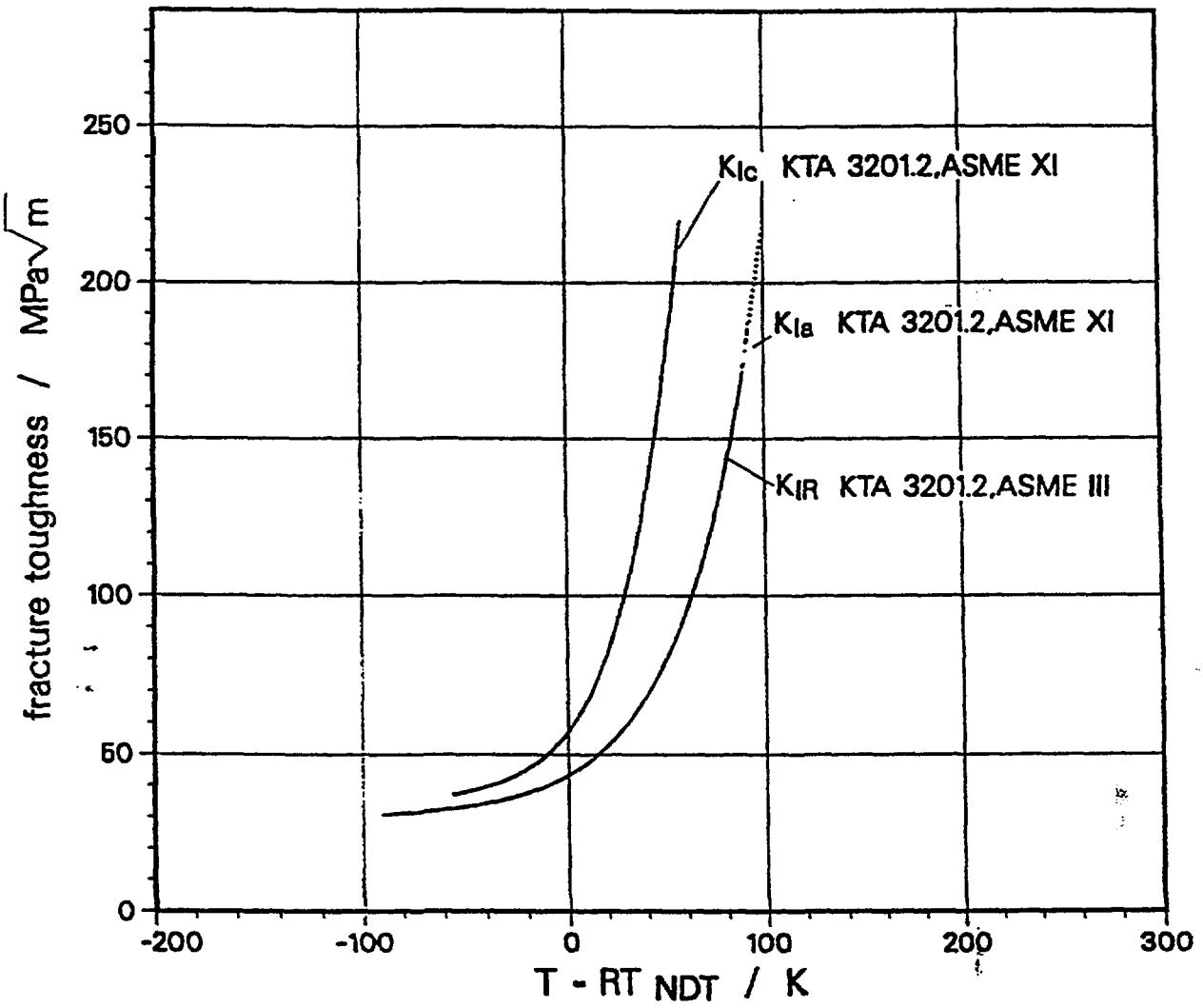
fracture toughness / MPa√m
250
200
150
100
50
0
-200
-100
0
100
200
300
T - RT NDT / K
KIc KTA 3201.2,ASME XI
KIa KTA 3201.2,ASME XI
KIR KTA 3201.2,ASME III

FIGURE 2

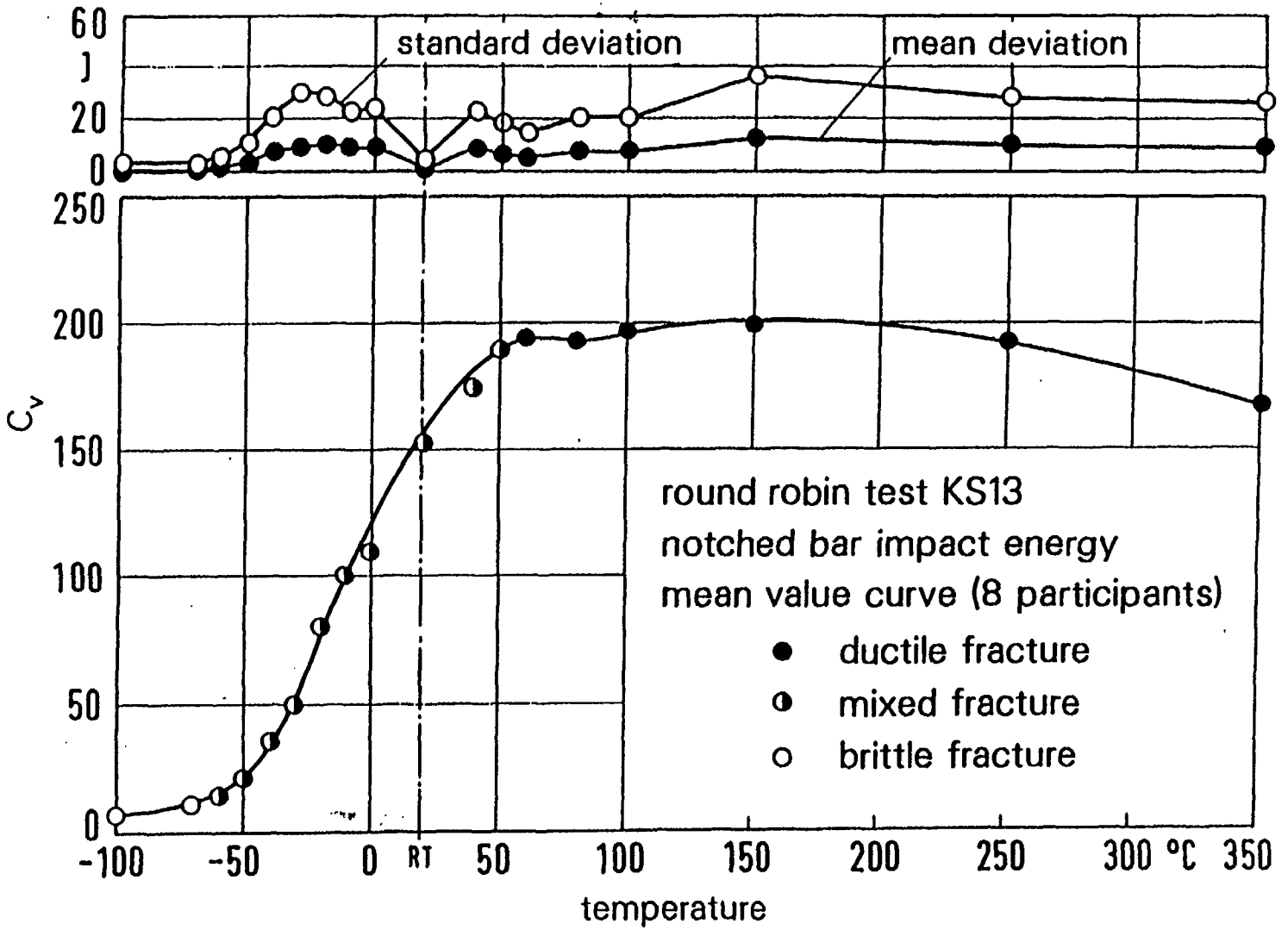
60
J
20
0
standard deviation
mean deviation
250
200
150
100
50
0
A_v
round robin test KS13
notched bar impact energy
mean value curve (8 participants)
ductile fracture
mixed fracture
brittle fracture
-100
-50
0
RT
50
100
150
200
250
300 °C
350
temperature

FIGURE 3

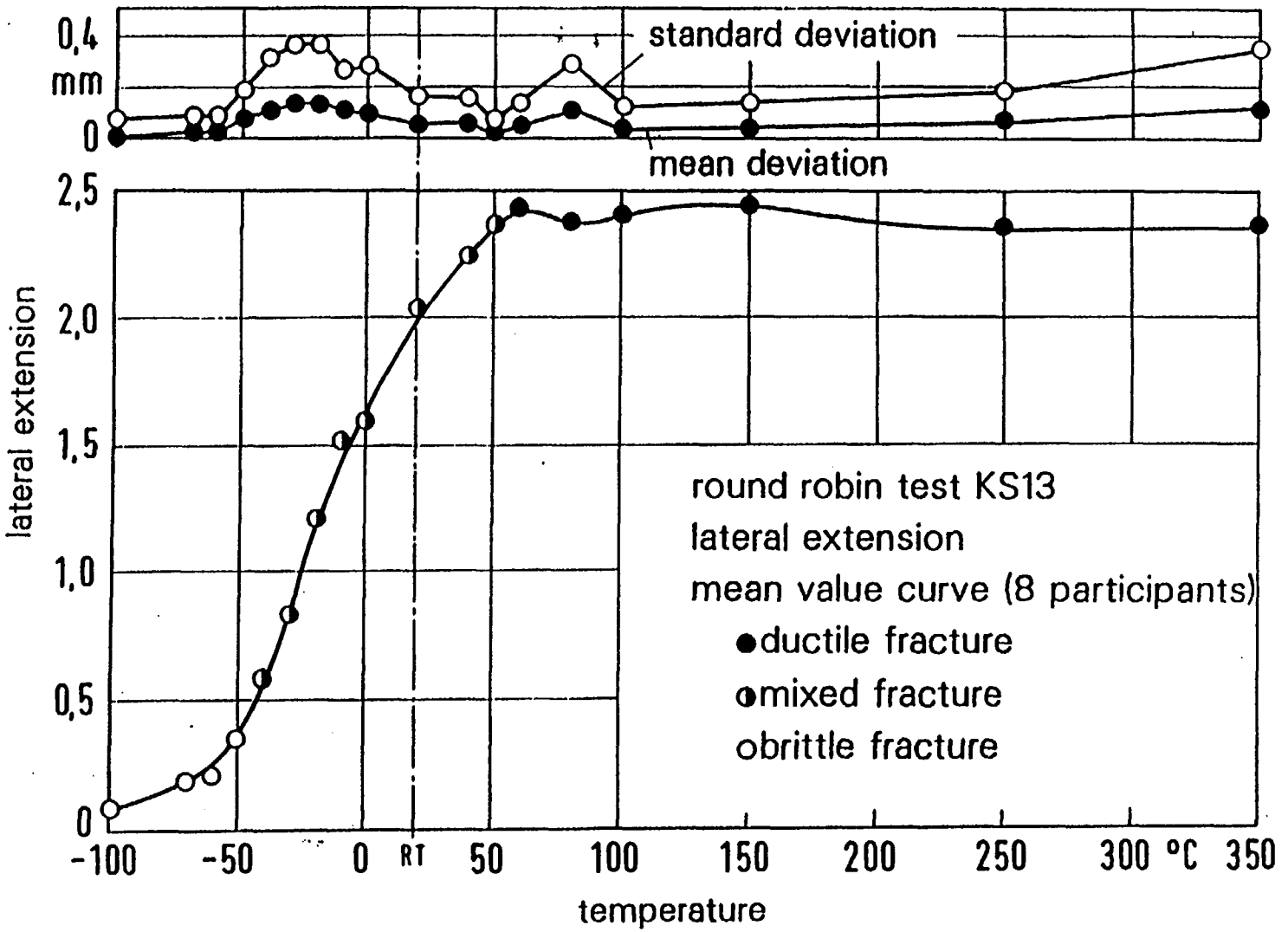
0,4
mm
0
standard deviation
mean deviation
2,5
2,0
1,5
1,0
0,5
0
lateral extension
round robin test KS13
lateral extension
mean value curve (8 participants)
●ductile fracture
◑mixed fracture
○brittle fracture
-100
-50
0
RT
50
100
150
200
250
300 °C
350
temperature

FIGURE 4

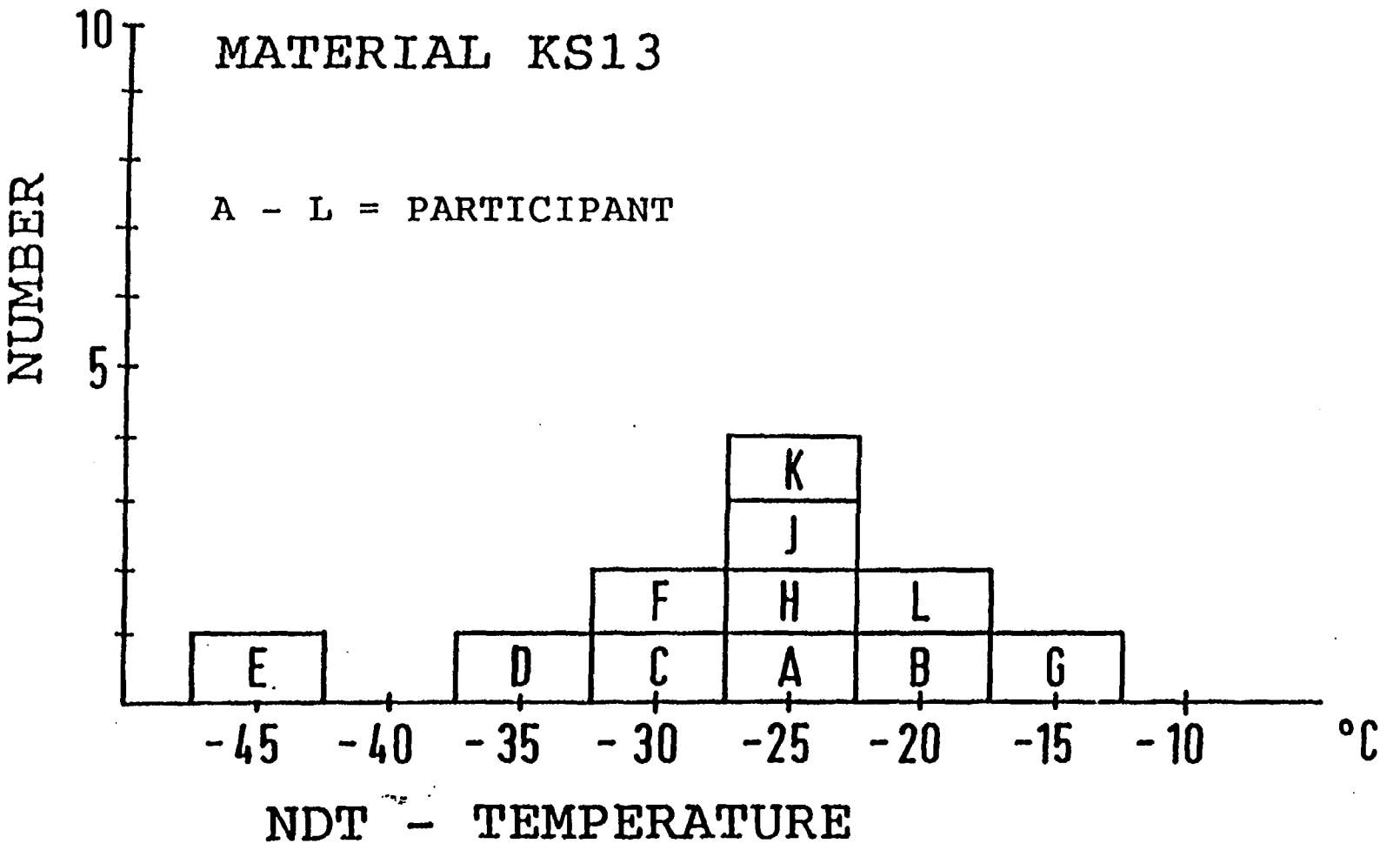
MATERIAL KS13
A - L = PARTICIPANT
NUMBER
10
5
K
J
F
H
L
E
D
C
A
B
G
-45
-40
-35
-30
-25
-20
-15
-10
°C
NDT - TEMPERATURE

FIGURE 5

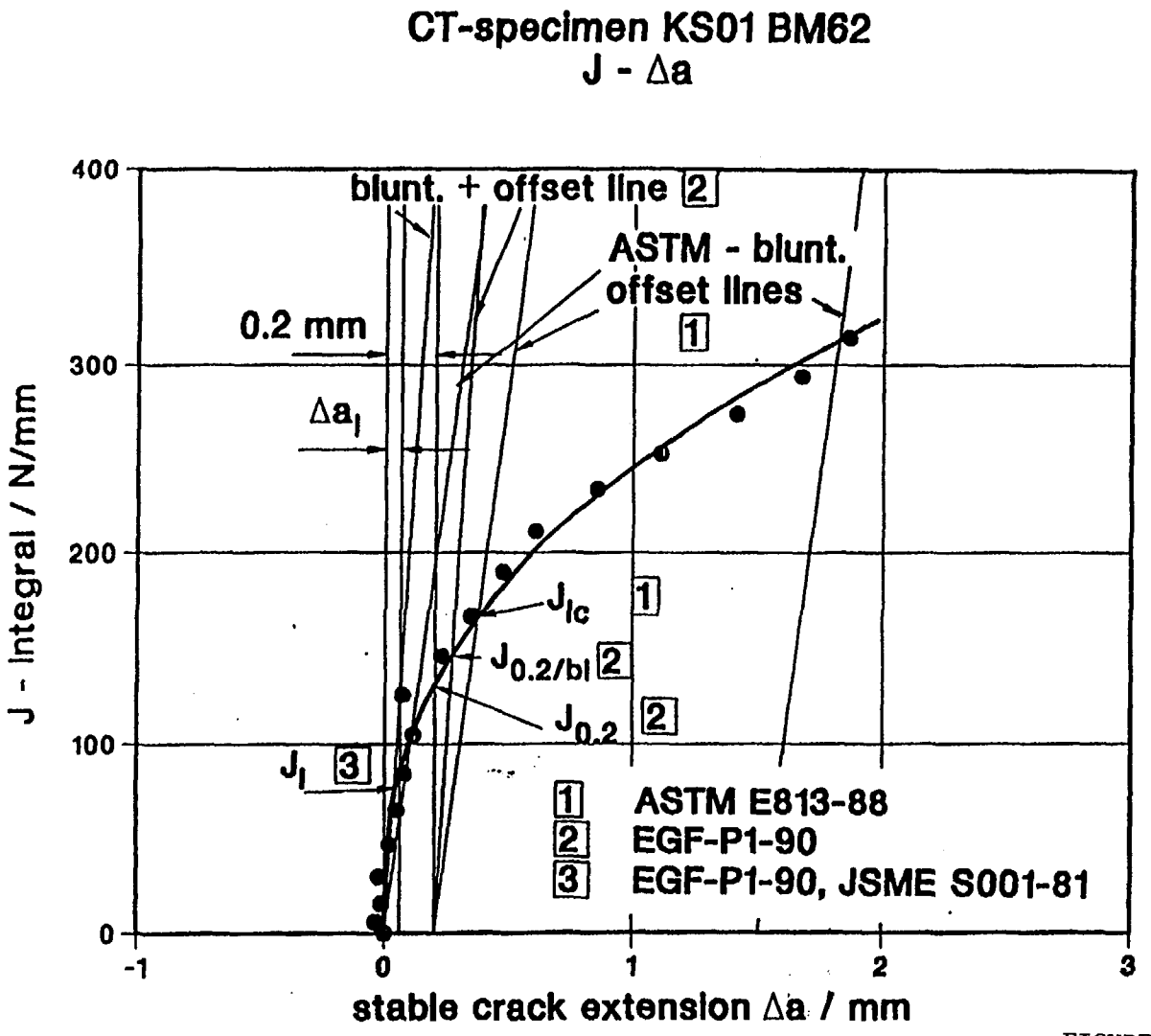
CT-specimen KS01 BM62
J - Δa
J - Integral / N/mm
stable crack extension Δa / mm
blunt. + offset line 2
ASTM - blunt.
offset lines
1
0.2 mm
Δa_I
J_Ic
1
J_0.2/bl 2
J_0.2 2
J_I 3
1 ASTM E813-88
2 EGF-P1-90
3 EGF-P1-90, JSME S001-81
400
300
200
100
0
-1
0
1
2
3

FIGURE 6

J–Integral / N/mm
0.0
50.0
100.0
150.0
J_i
exp.blunting line
Δa_i
Δa / mm
0.0
0.2
0.4
0.6
0.8
1.0
1.2
1.4
1.6
1.8
2.0
J
J_i
Δa_i
Δa

FIGURE 7

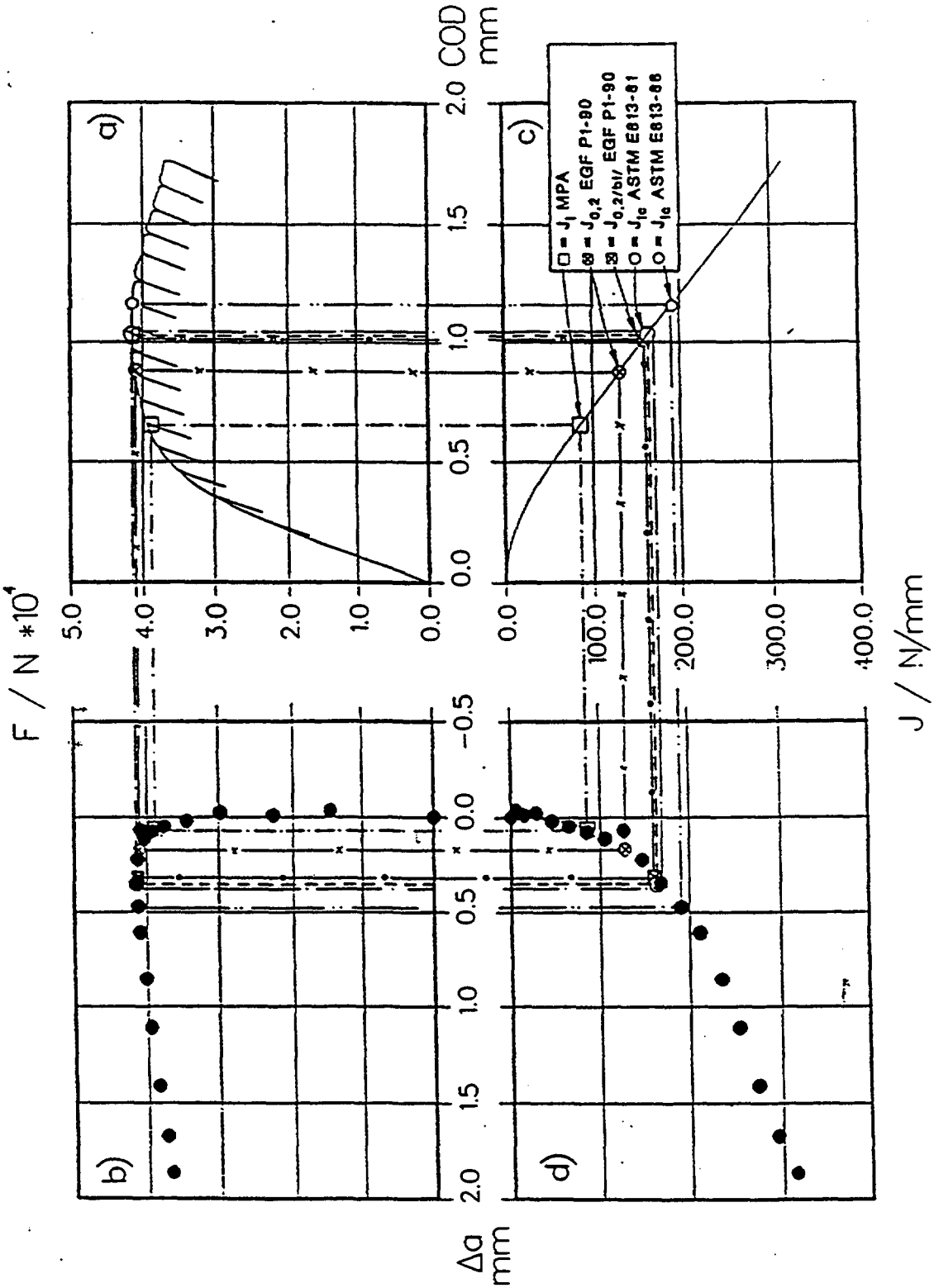
a)
b)
c)
d)
F / N *10⁴
COD mm
Δa mm
J / N/mm
□ = J_I MPA
▨ = J_0,2 EGF P1-90
▨ = J_0,2/bl/ EGF P1-90
○ = J_Ic ASTM E813-81
○ = J_Ic ASTM E813-86

FIGURE 8

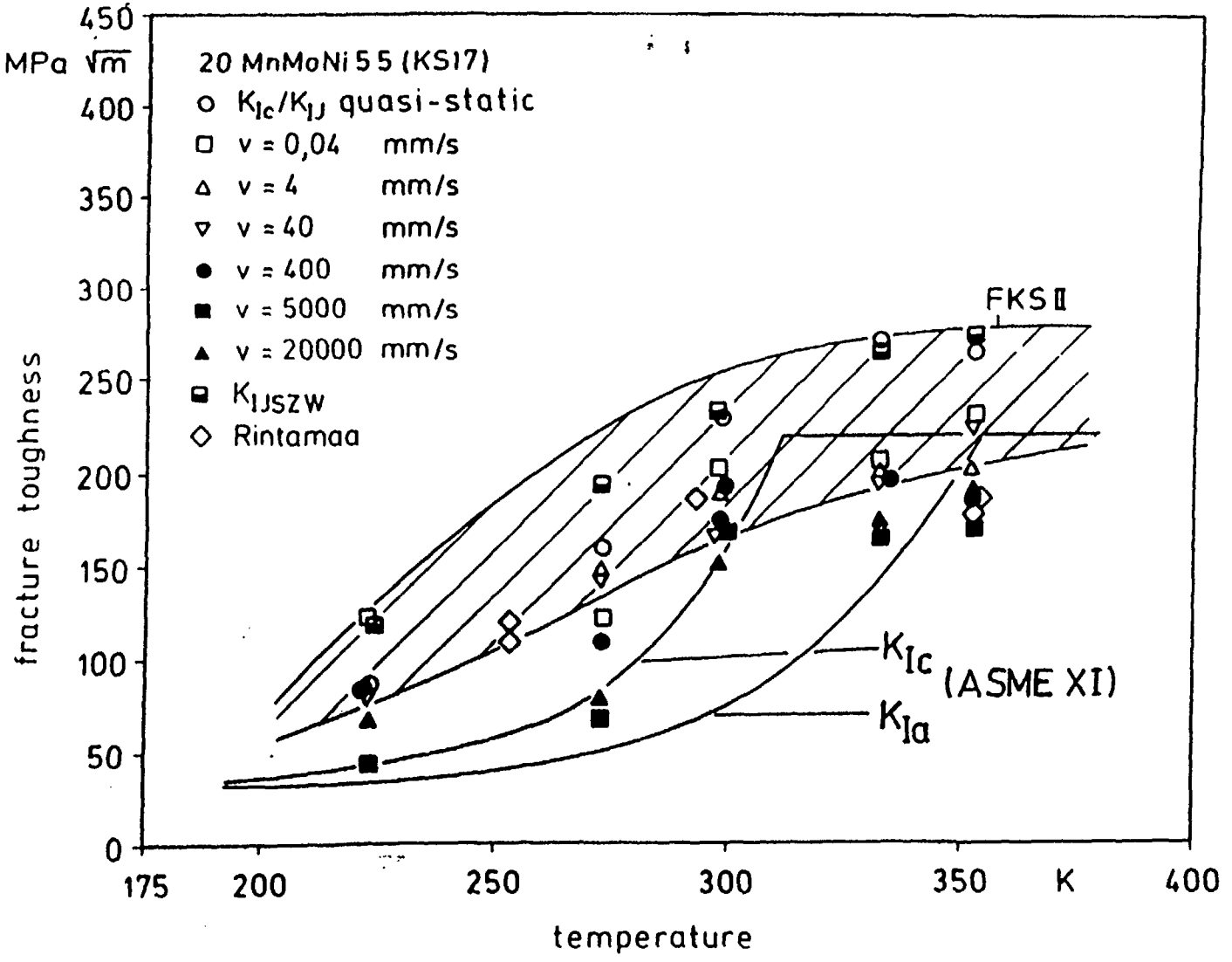
MPa √m
fracture toughness
temperature
20 MnMoNi 5 5 (KS17)
o K_{Ic}/K_{IJ} quasi-static
□ v = 0,04 mm/s
△ v = 4 mm/s
▽ v = 40 mm/s
● v = 400 mm/s
■ v = 5000 mm/s
▲ v = 20000 mm/s
◘ K_{IJSZW}
◇ Rintamaa
FKS II
K_{Ic} (ASME XI)
K_{Ia}
450
400
350
300
250
200
150
100
50
0
175
200
250
300
350
K
400

FIGURE 9

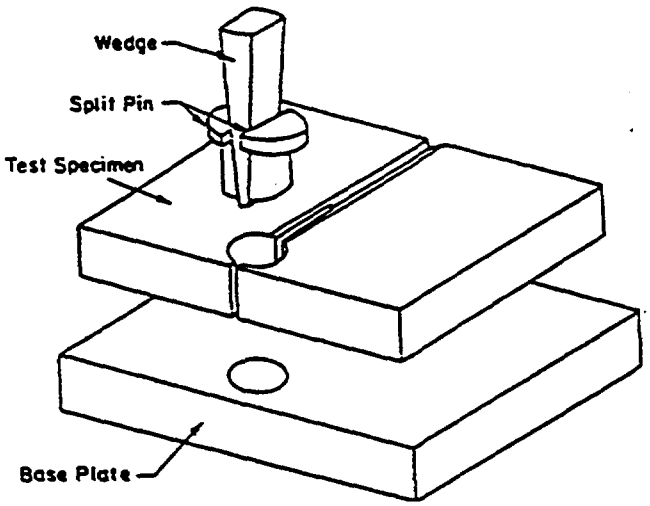

FIGURE 10

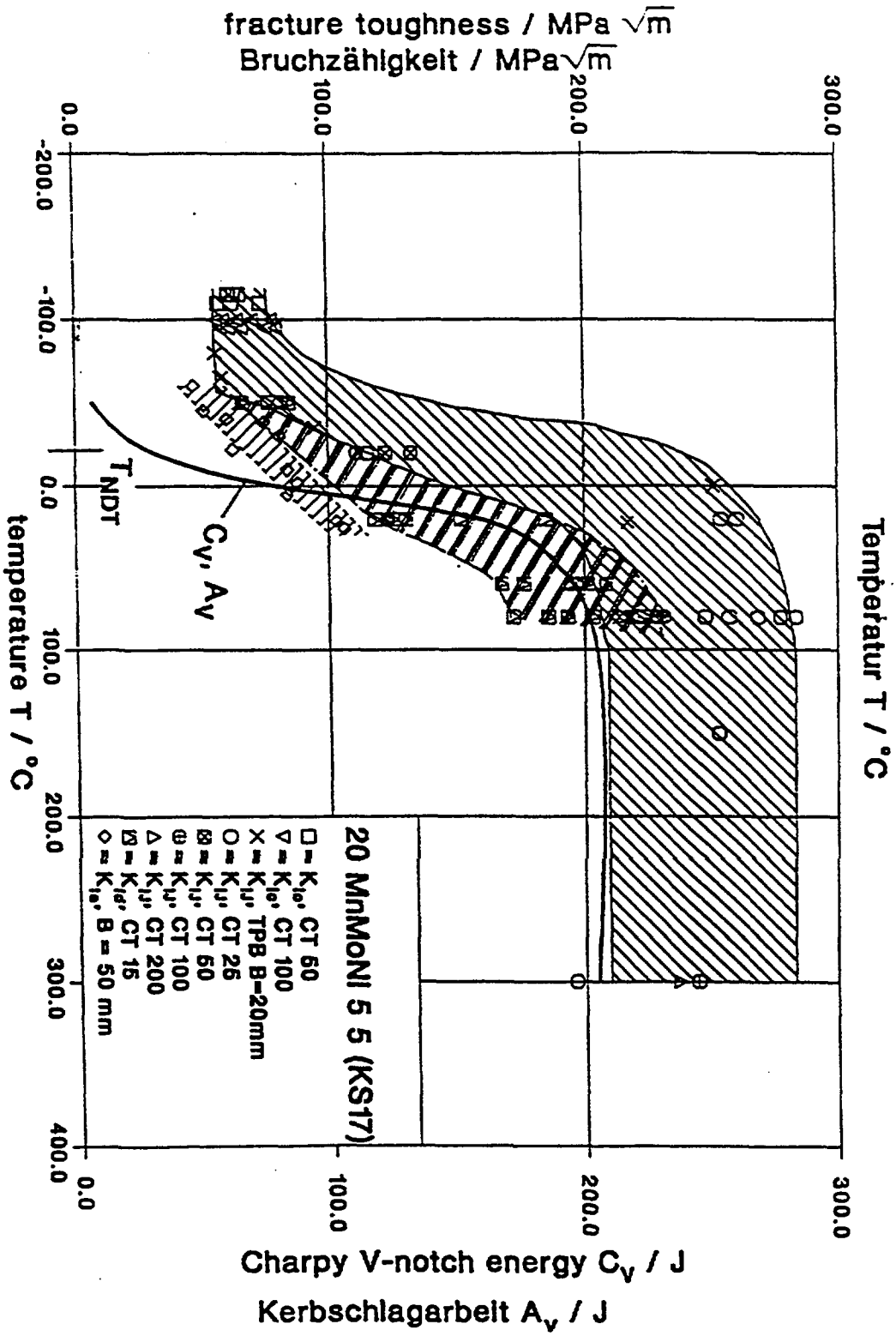
fracture toughness / MPa √m
Bruchzähigkeit / MPa√m
0.0
100.0
200.0
300.0
-200.0
-100.0
0.0
100.0
200.0
300.0
400.0
temperature T / °C
Temperatur T / °C
T_NDT
C_V, A_V
20 MnMoNi 5 5 (KS17)
□ = K_Ic, CT 50
▽ = K_Ic, CT 100
× = K_Ic, TPB B=20mm
○ = K_Id, CT 25
⊠ = K_Id, CT 50
⊕ = K_Id, CT 100
△ = K_Id, CT 200
⊡ = K_Id, CT 15
◇ = K_Id, B = 50 mm
Charpy V-notch energy C_V / J
Kerbschlagarbeit A_V / J

FIGURE 11

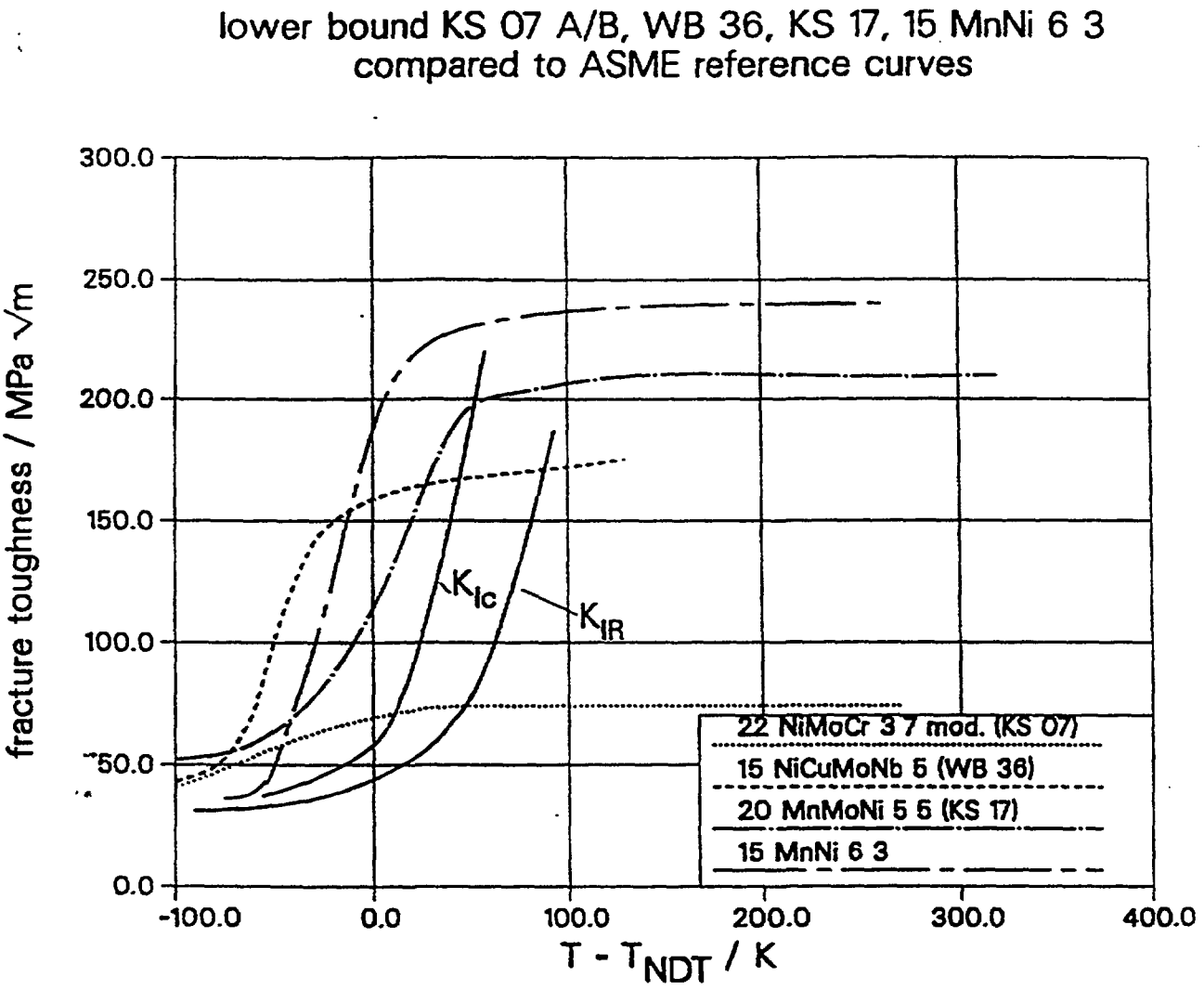
lower bound KS 07 A/B, WB 36, KS 17, 15 MnNi 6 3
compared to ASME reference curves
fracture toughness / MPa √m
300.0
250.0
200.0
150.0
100.0
50.0
0.0
-100.0
0.0
100.0
200.0
300.0
400.0
T - T_NDT / K
K_Ic
K_IR
22 NiMoCr 3 7 mod. (KS 07)
15 NiCuMoNb 5 (WB 36)
20 MnMoNi 5 5 (KS 17)
15 MnNi 6 3

FIGURE 12

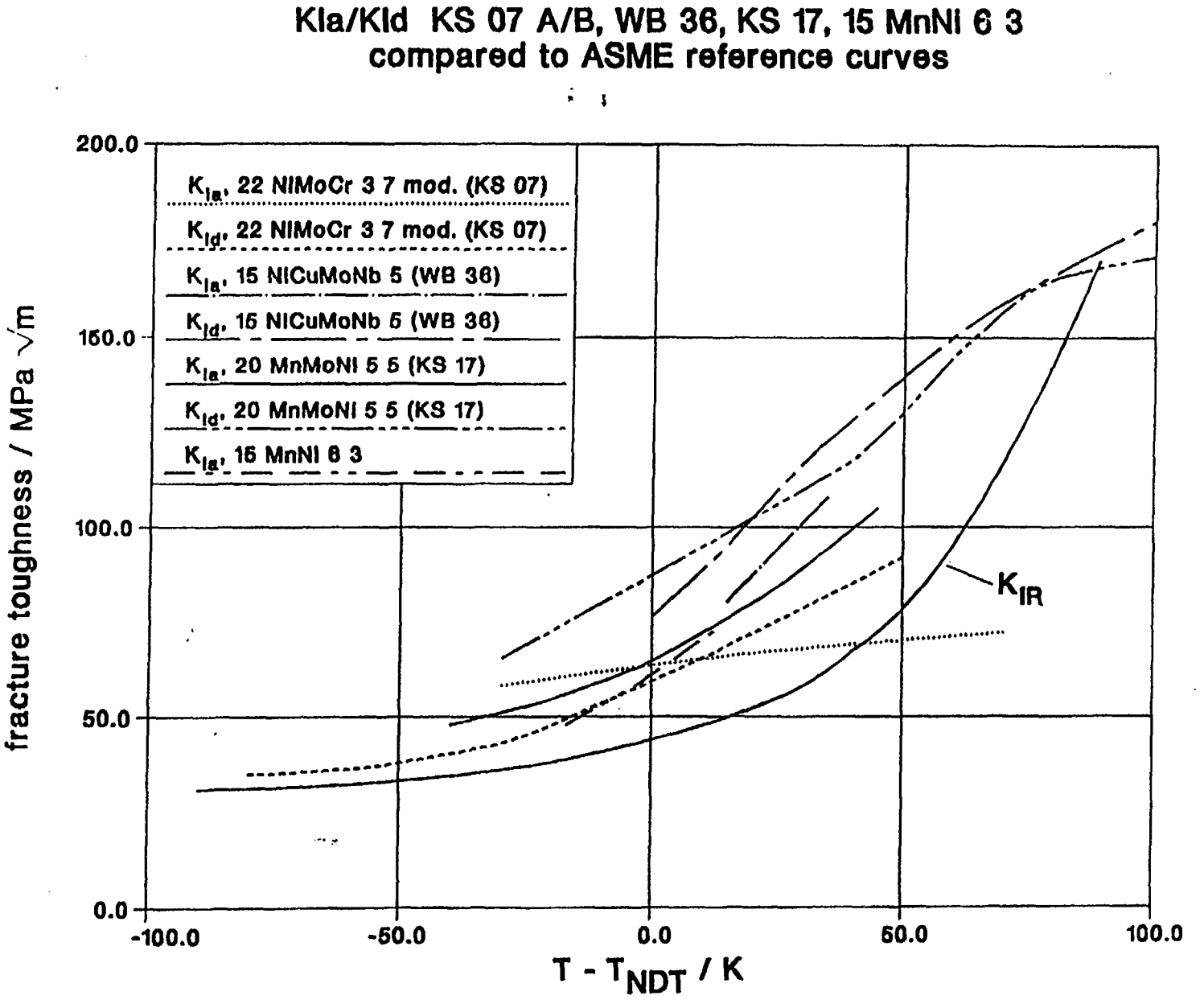
Kla/Kld KS 07 A/B, WB 36, KS 17, 15 MnNi 6 3
compared to ASME reference curves
K_{Ia}, 22 NiMoCr 3 7 mod. (KS 07)
K_{Id}, 22 NiMoCr 3 7 mod. (KS 07)
K_{Ia}, 15 NiCuMoNb 5 (WB 36)
K_{Id}, 15 NiCuMoNb 5 (WB 36)
K_{Ia}, 20 MnMoNi 5 5 (KS 17)
K_{Id}, 20 MnMoNi 5 5 (KS 17)
K_{Ia}, 15 MnNi 6 3
K_{IR}
fracture toughness / MPa √m
200.0
150.0
100.0
50.0
0.0
-100.0
-50.0
0.0
50.0
100.0
T - T_{NDT} / K

FIGURE 13

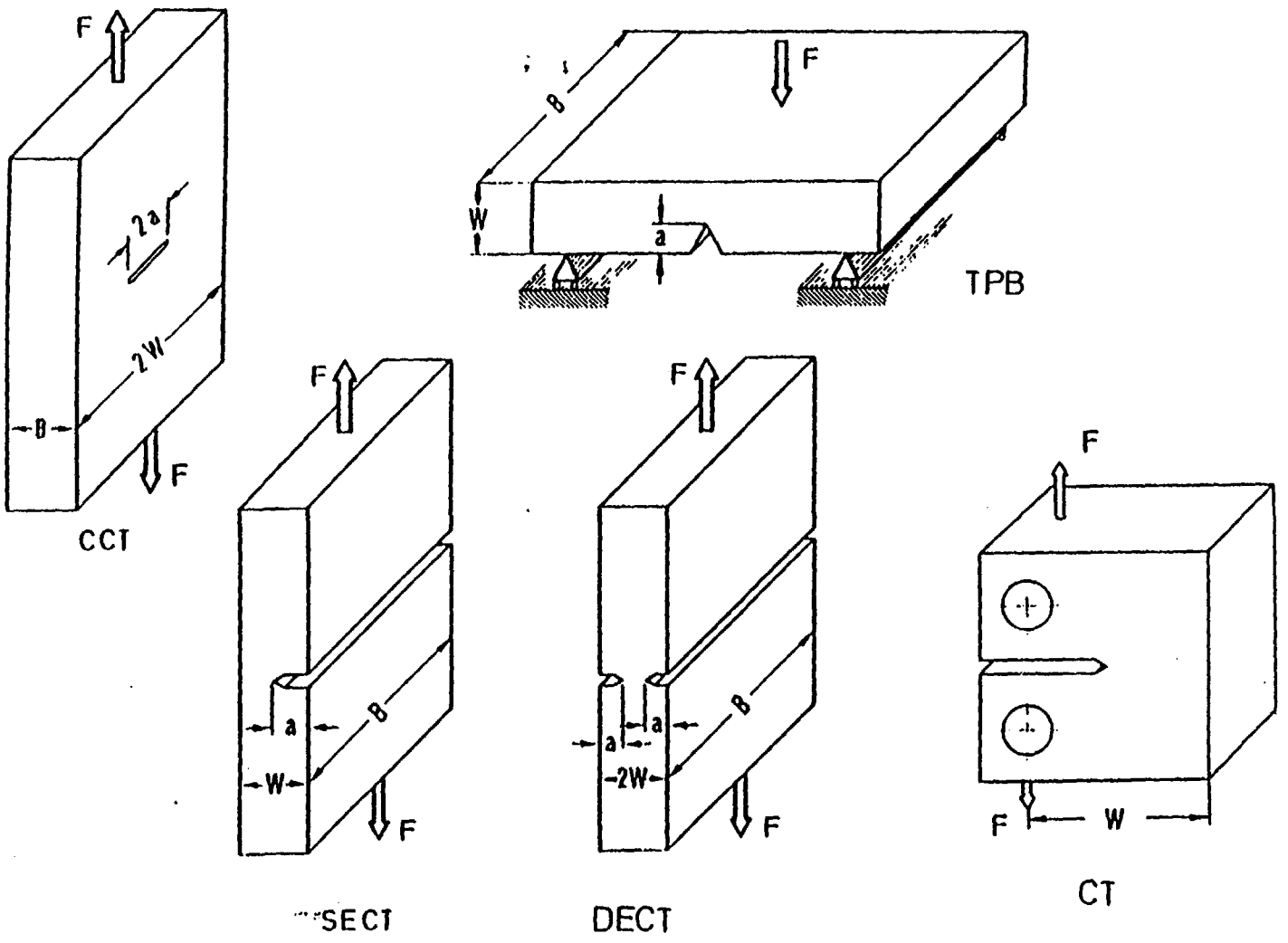

FIGURE 14

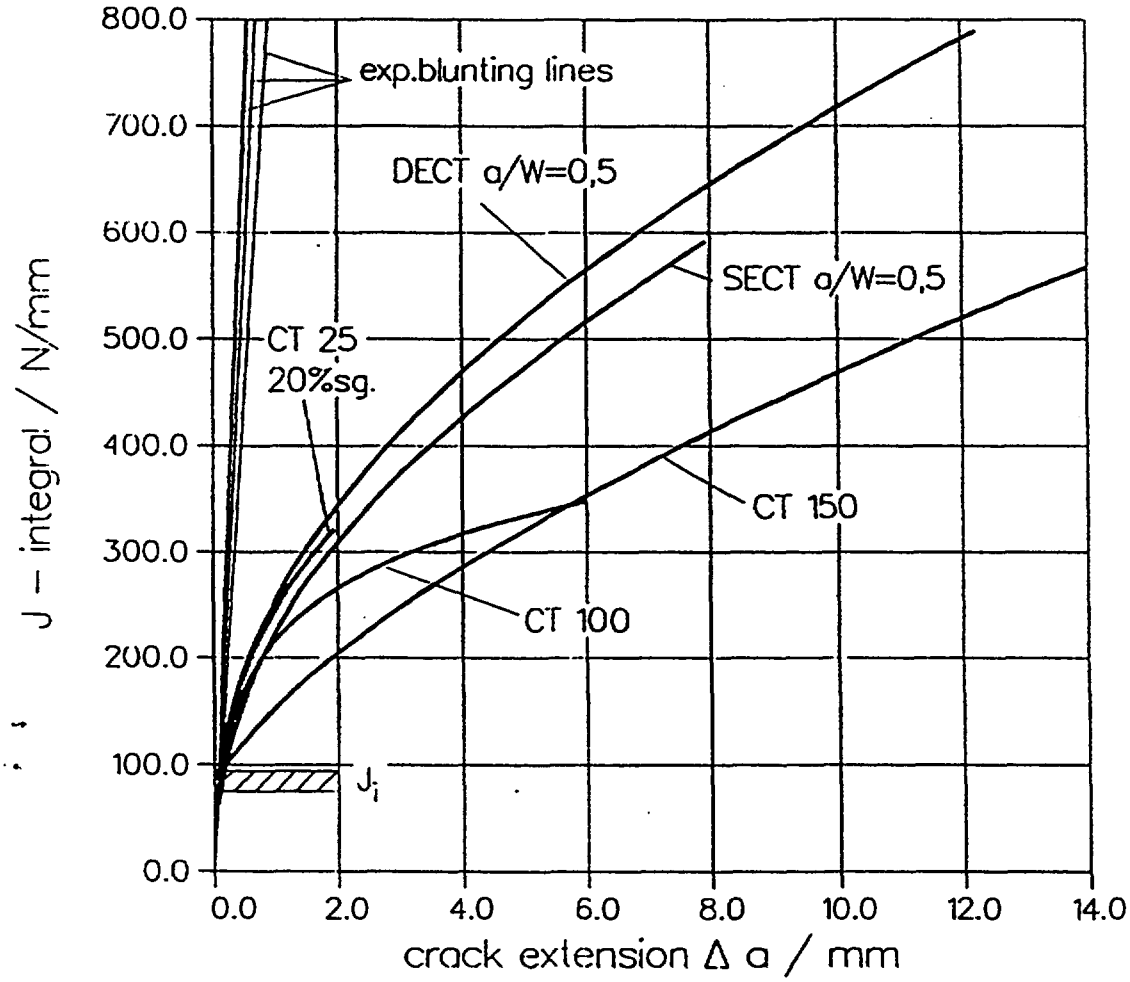
800.0
700.0
600.0
500.0
400.0
300.0
200.0
100.0
0.0
J – integral / N/mm
exp.blunting lines
DECT a/W=0,5
SECT a/W=0,5
CT 25
20%sg.
CT 150
CT 100
J_i
0.0
2.0
4.0
6.0
8.0
10.0
12.0
14.0
crack extension Δ a / mm

FIGURE 15 a

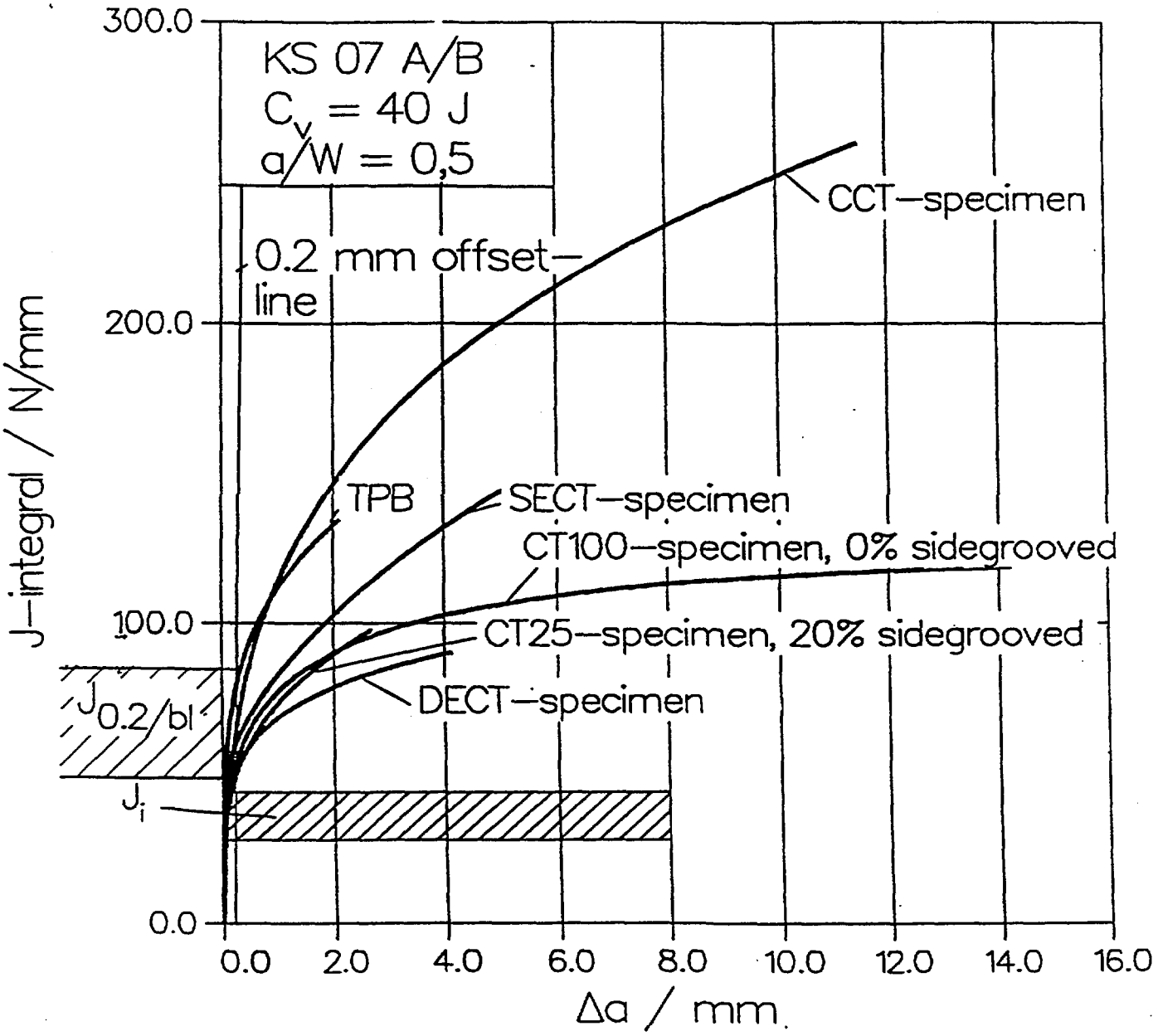
KS 07 A/B
C_v = 40 J
a/W = 0,5
0.2 mm offset–line
CCT–specimen
TPB
SECT–specimen
CT100–specimen, 0% sidegrooved
CT25–specimen, 20% sidegrooved
DECT–specimen
$J_{0.2/bl}$
J_i
J–integral / N/mm
Δa / mm
300.0
200.0
100.0
0.0
0.0
2.0
4.0
6.0
8.0
10.0
12.0
14.0
16.0

FIGURE 15 b

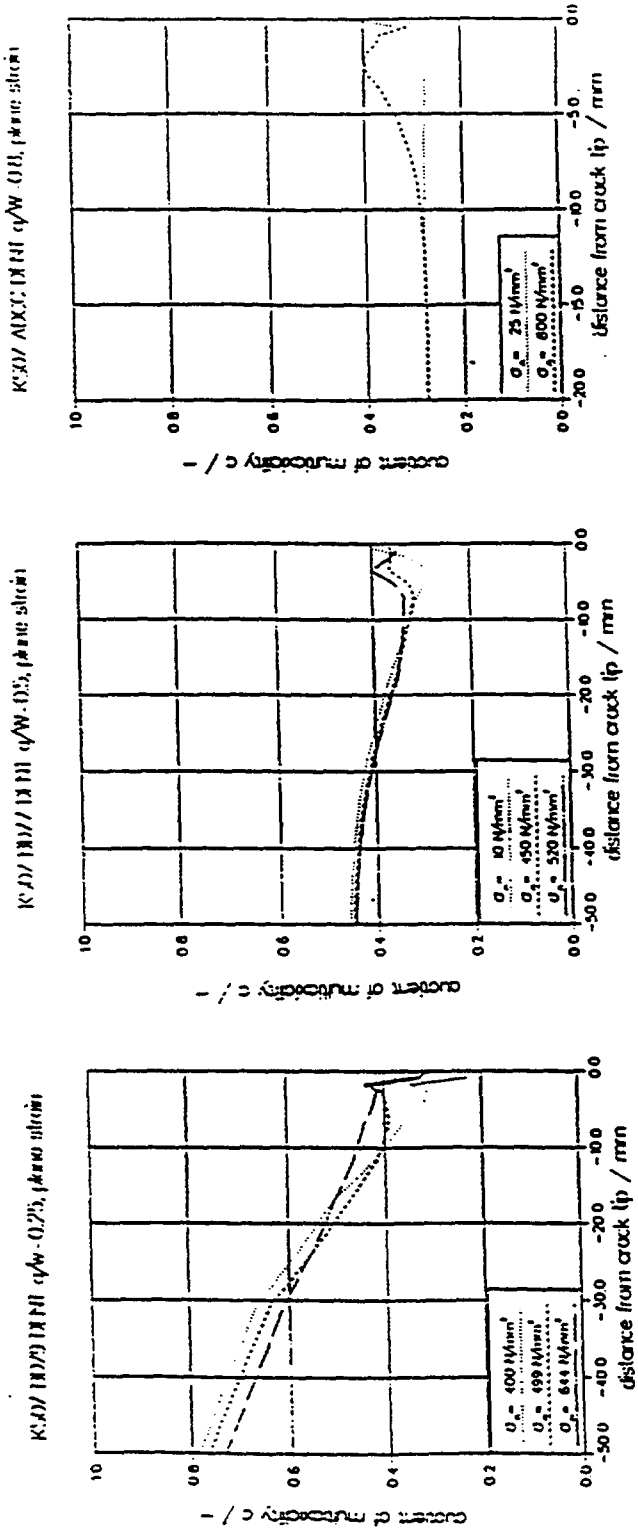
degree of multiaxiality c / –
distance from crack tip / mm
0.0
-10.0
-20.0
-30.0
-40.0
-50.0
0.2
0.4
0.6
0.8
1.0

FIGURE 16

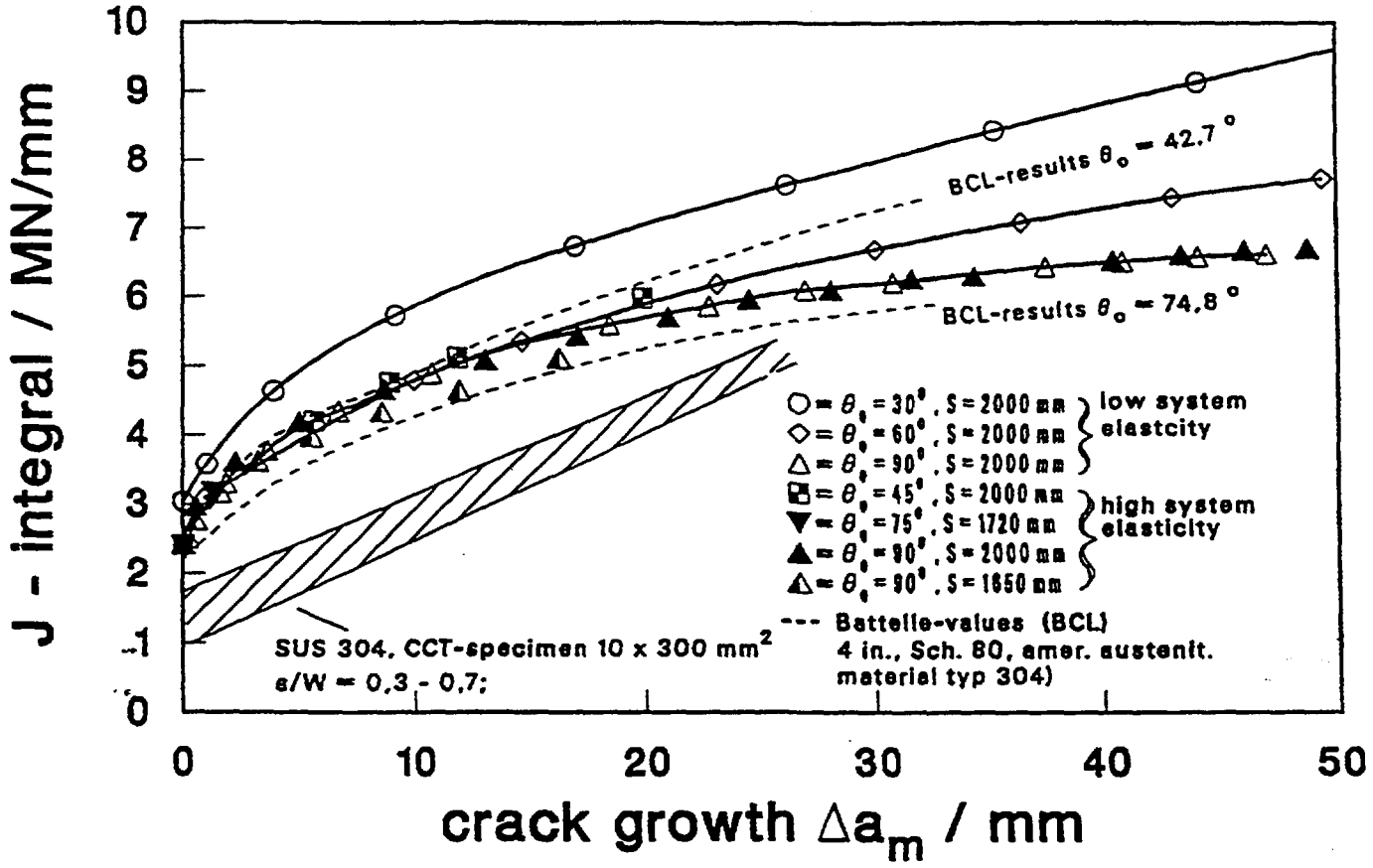
J - integral / MN/mm
crack growth Δa_m / mm
BCL-results θ_o = 42.7 °
BCL-results θ_o = 74.8 °
low system elastcity
high system elasticity
S = 2000 mm
S = 1720 mm
S = 1650 mm
Battelle-values (BCL)
4 in., Sch. 80, amer. austenit. material typ 304)
SUS 304, CCT-specimen 10 x 300 mm²
a/W = 0,3 - 0,7;

FIGURE 17

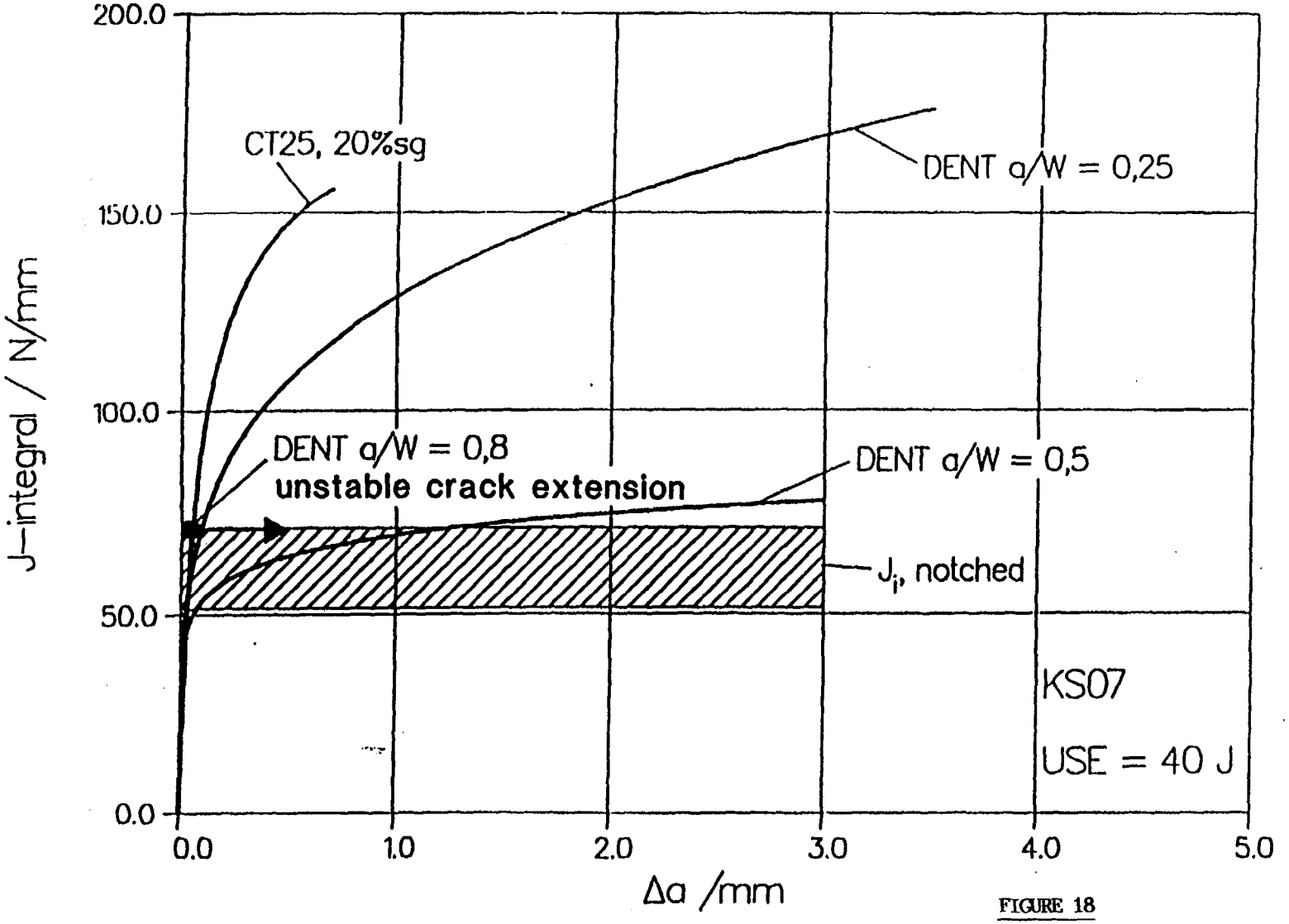
200.0
150.0
100.0
50.0
0.0
J-integral / N/mm
CT25, 20%sg
DENT a/W = 0,25
DENT a/W = 0,8
unstable crack extension
DENT a/W = 0,5
J_i, notched
KS07
USE = 40 J
0.0
1.0
2.0
3.0
4.0
5.0
Δa /mm

FIGURE 18

Wall thickness s

s=148mm

long. crack

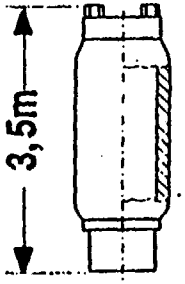

ORNL

s=200mm

circ.f. crack

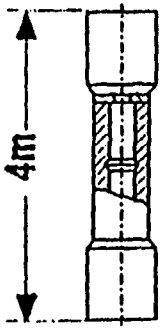

MPA

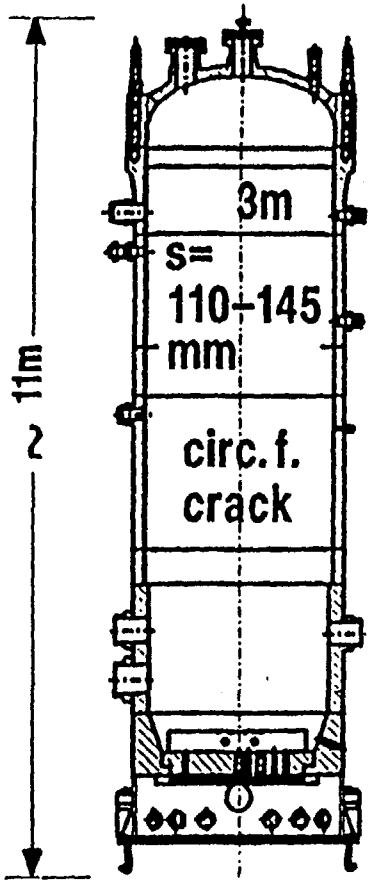

HDR

FIGURE 19

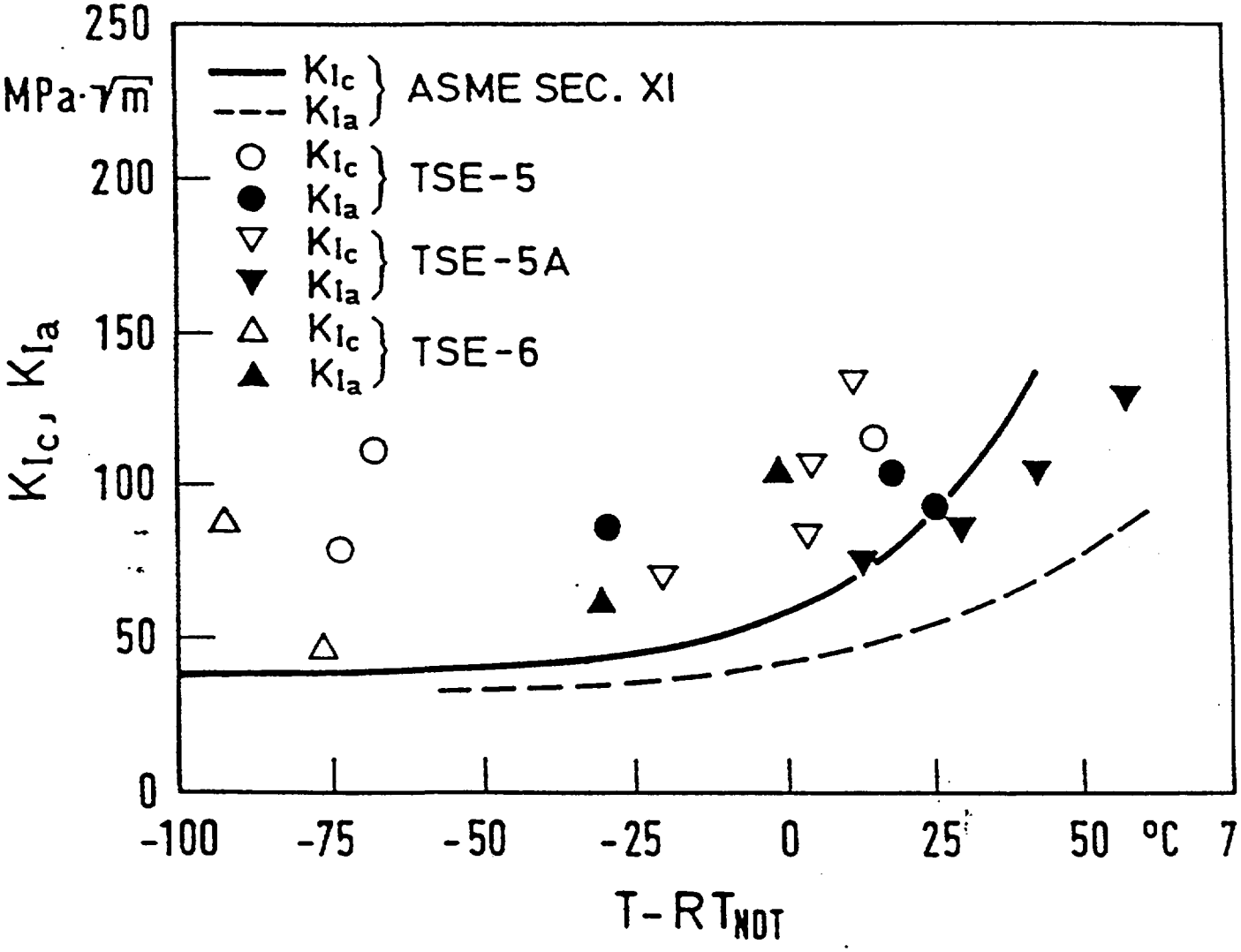
250
MPa·√m
200
150
100
50
0
K_{Ic}, K_{Ia}
K_{Ic}
K_{Ia}
ASME SEC. XI
TSE-5
TSE-5A
TSE-6
-100
-75
-50
-25
0
25
50
°C
T-RT$_{NDT}$

FIGURE 20

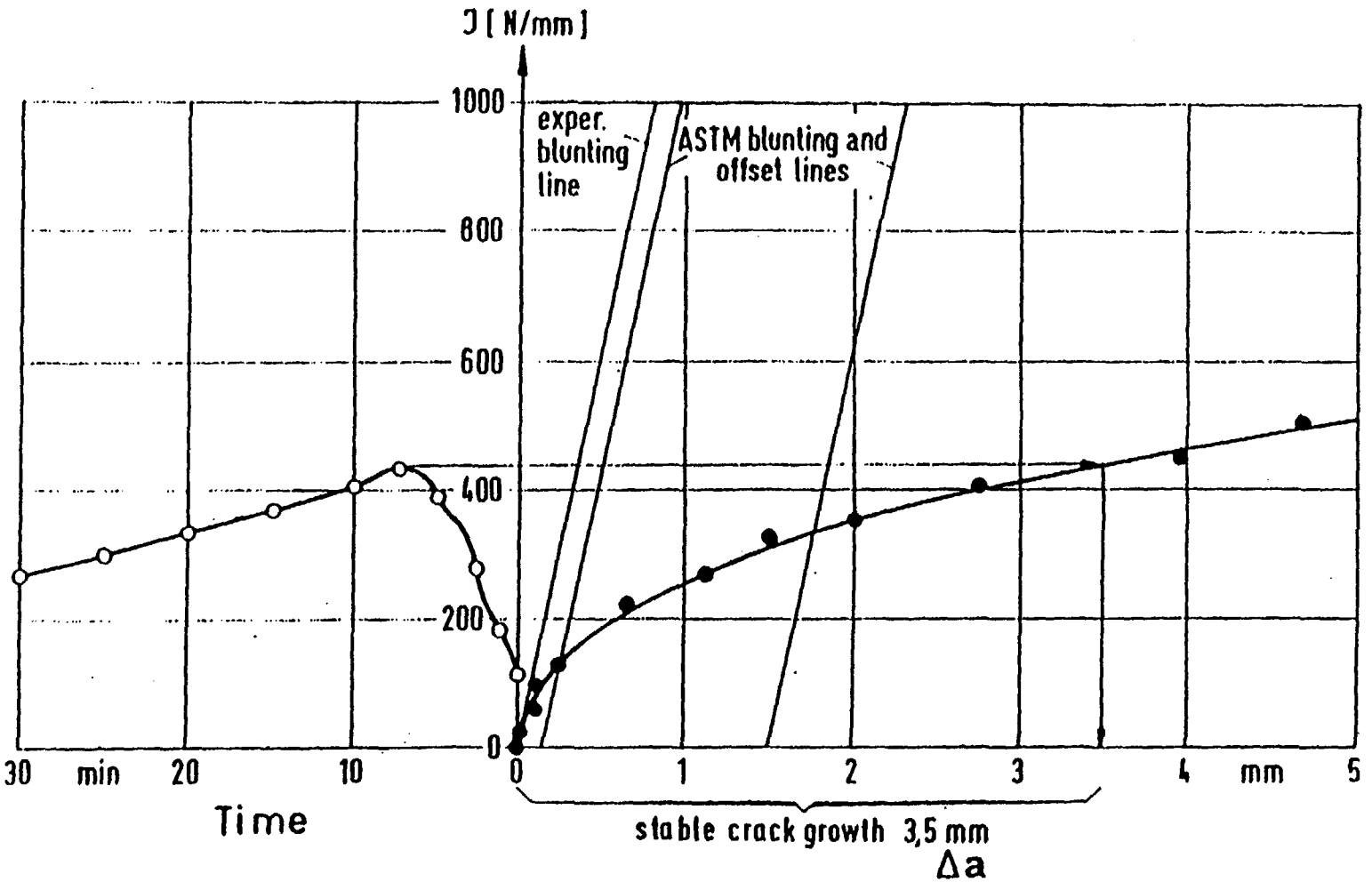
J [N/mm]
1000
800
600
400
200
0
exper. blunting line
ASTM blunting and offset lines
30 min 20 10 0 1 2 3 4 mm 5
Time
stable crack growth 3,5 mm
Δa

FIGURE 21

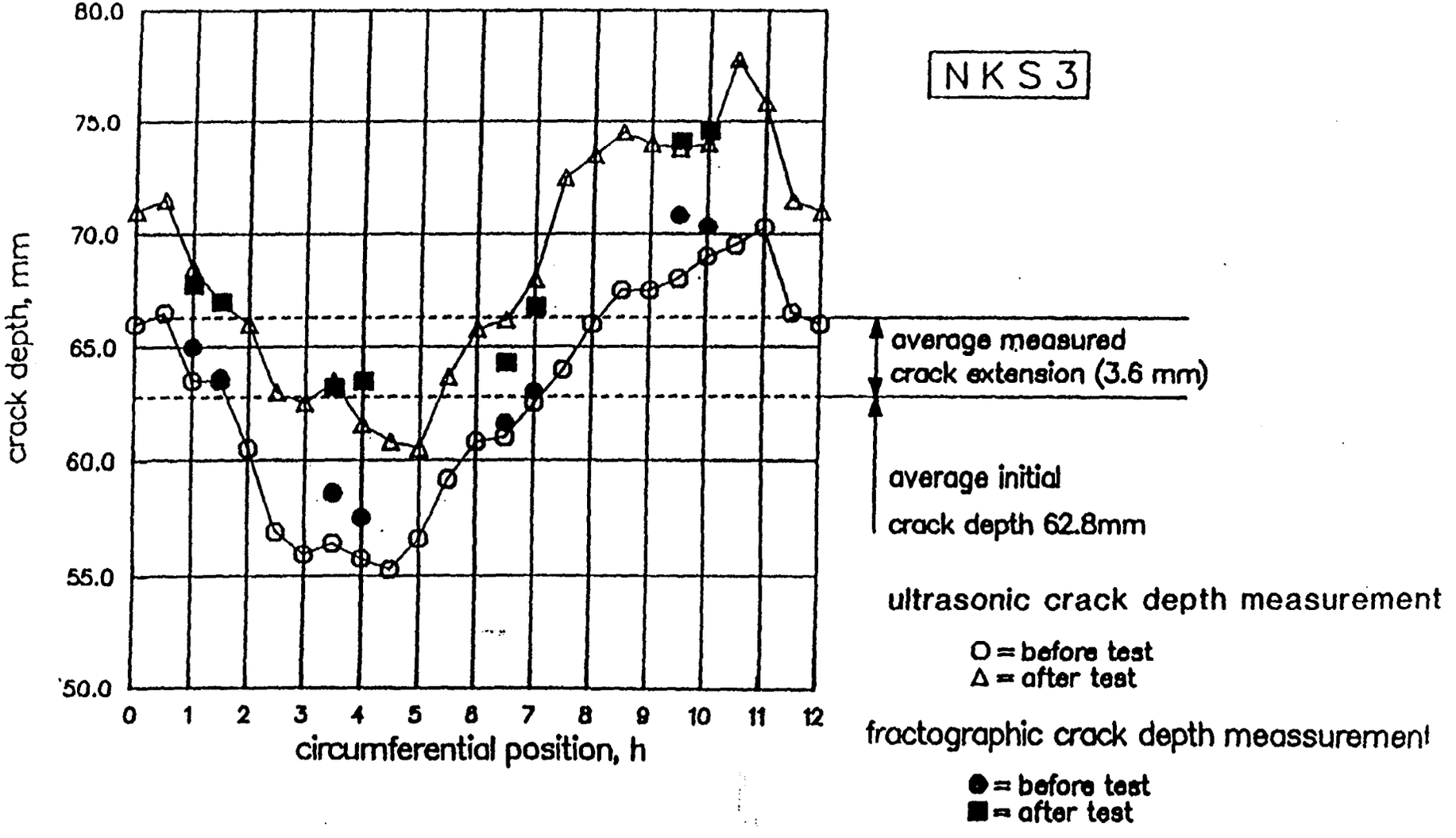
NKS 3
80.0
75.0
70.0
65.0
60.0
55.0
50.0
crack depth, mm
0 1 2 3 4 5 6 7 8 9 10 11 12
circumferential position, h
average measured
crack extension (3.6 mm)
average initial
crack depth 62.8mm
ultrasonic crack depth measurement
O = before test
Δ = after test
fractographic crack depth meassurement
● = before test
■ = after test

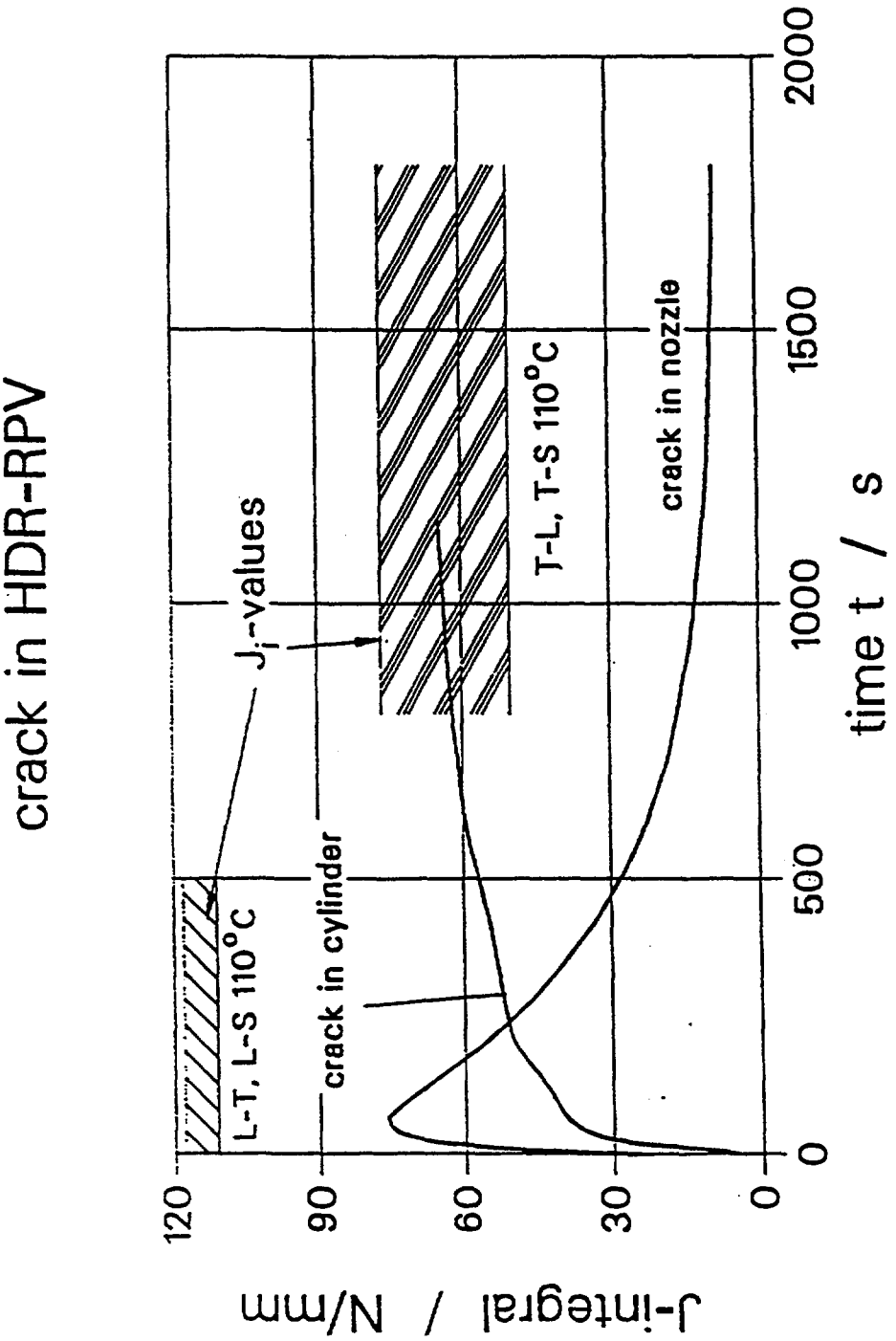
crack in HDR-RPV
J-integral / N/mm
time t / s
0
30
60
90
120
0
500
1000
1500
2000
L-T, L-S 110°C
crack in cylinder
J_i-values
T-L, T-S 110°C
crack in nozzle

FIGURE 23

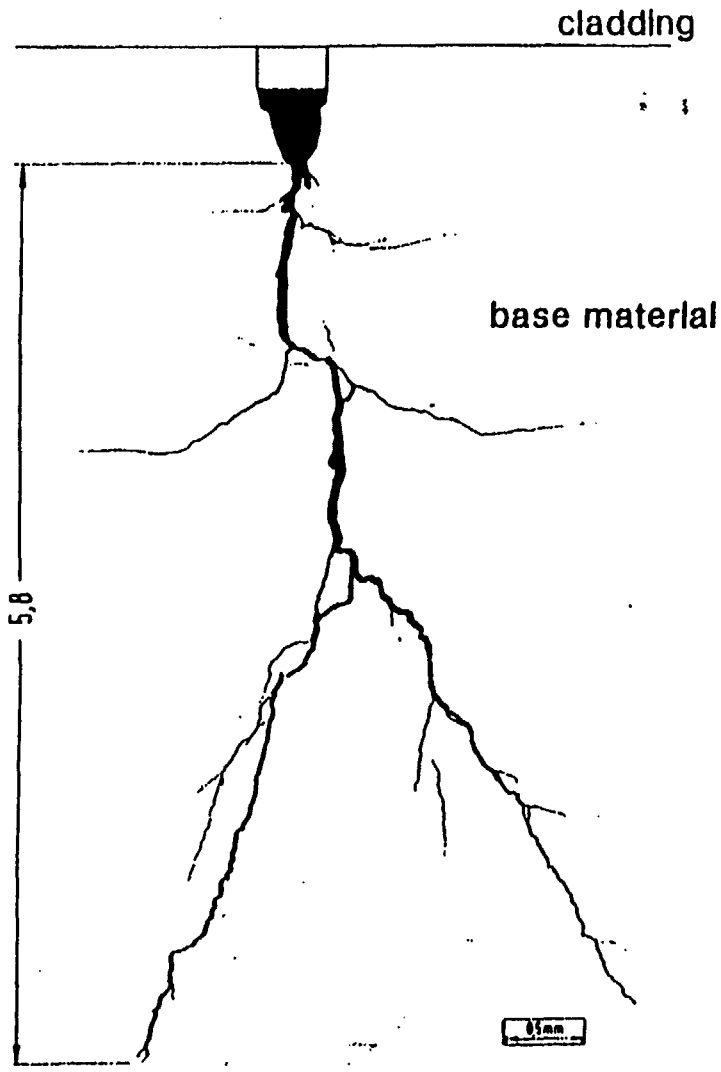

section A from B9 S1

Typical Branching of the Cracks

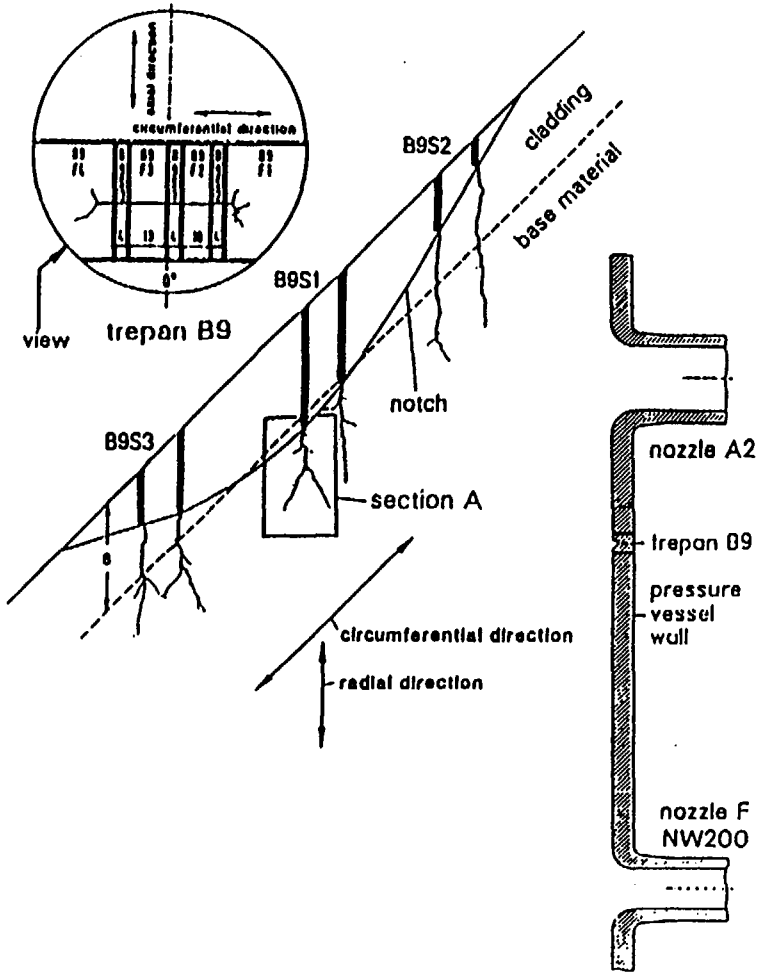

section from HDR trepan B9

Section of a Crack in the RPV-Cylinder

FIGURE 24

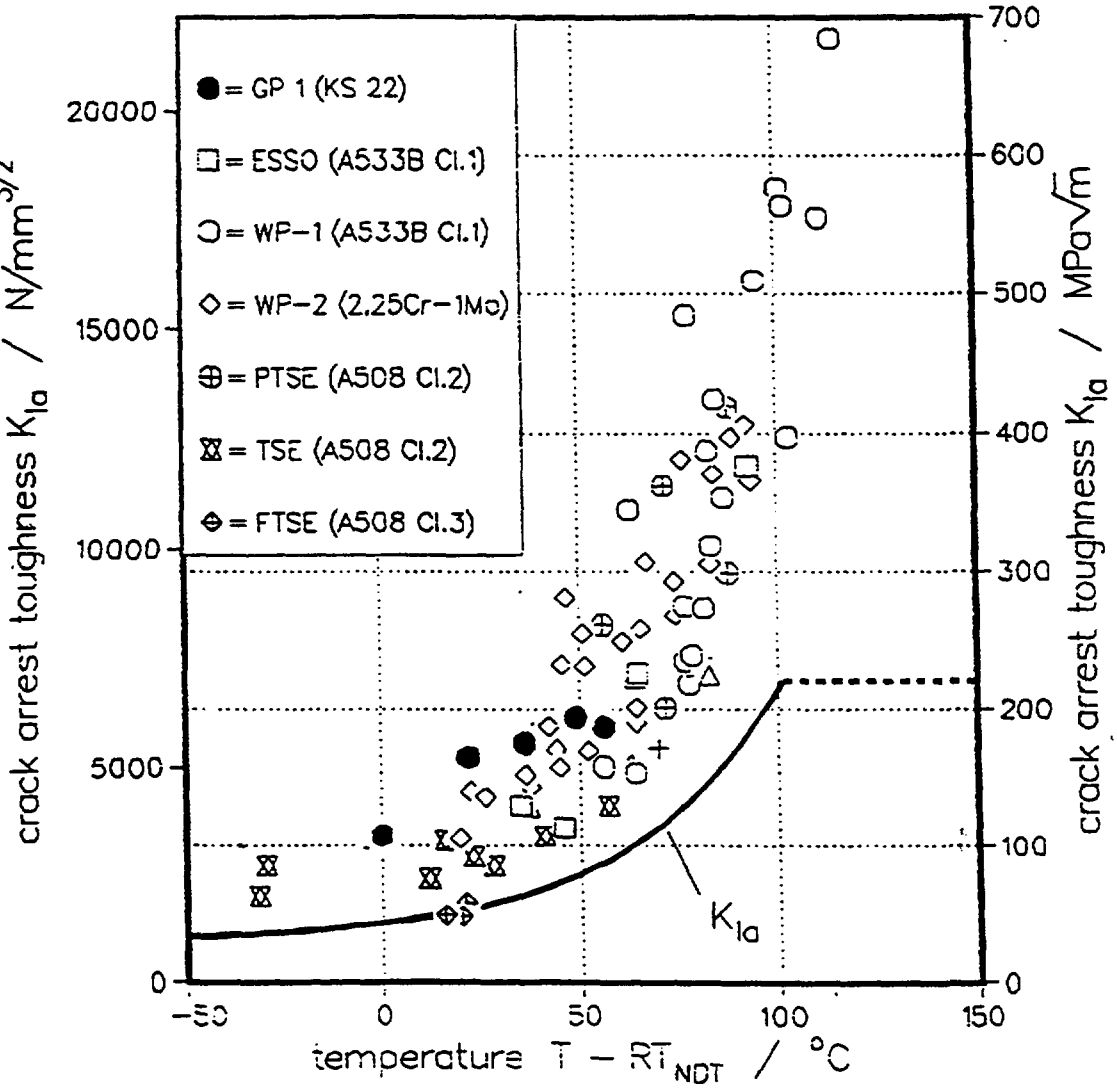
● = GP 1 (KS 22)
□ = ESSO (A533B Cl.1)
○ = WP-1 (A533B Cl.1)
◇ = WP-2 (2.25Cr-1Mo)
⊕ = PTSE (A508 Cl.2)
⊠ = TSE (A508 Cl.2)
⊖ = FTSE (A508 Cl.3)
crack arrest toughness K_{Ia} / N/mm$^{3/2}$
crack arrest toughness K_{Ia} / MPa$\sqrt{m}$
K_{Ia}
temperature $T - RT_{NDT}$ / °C
20000
15000
10000
5000
0
700
600
500
400
300
200
100
0
-50
0
50
100
150

FIGURE 25

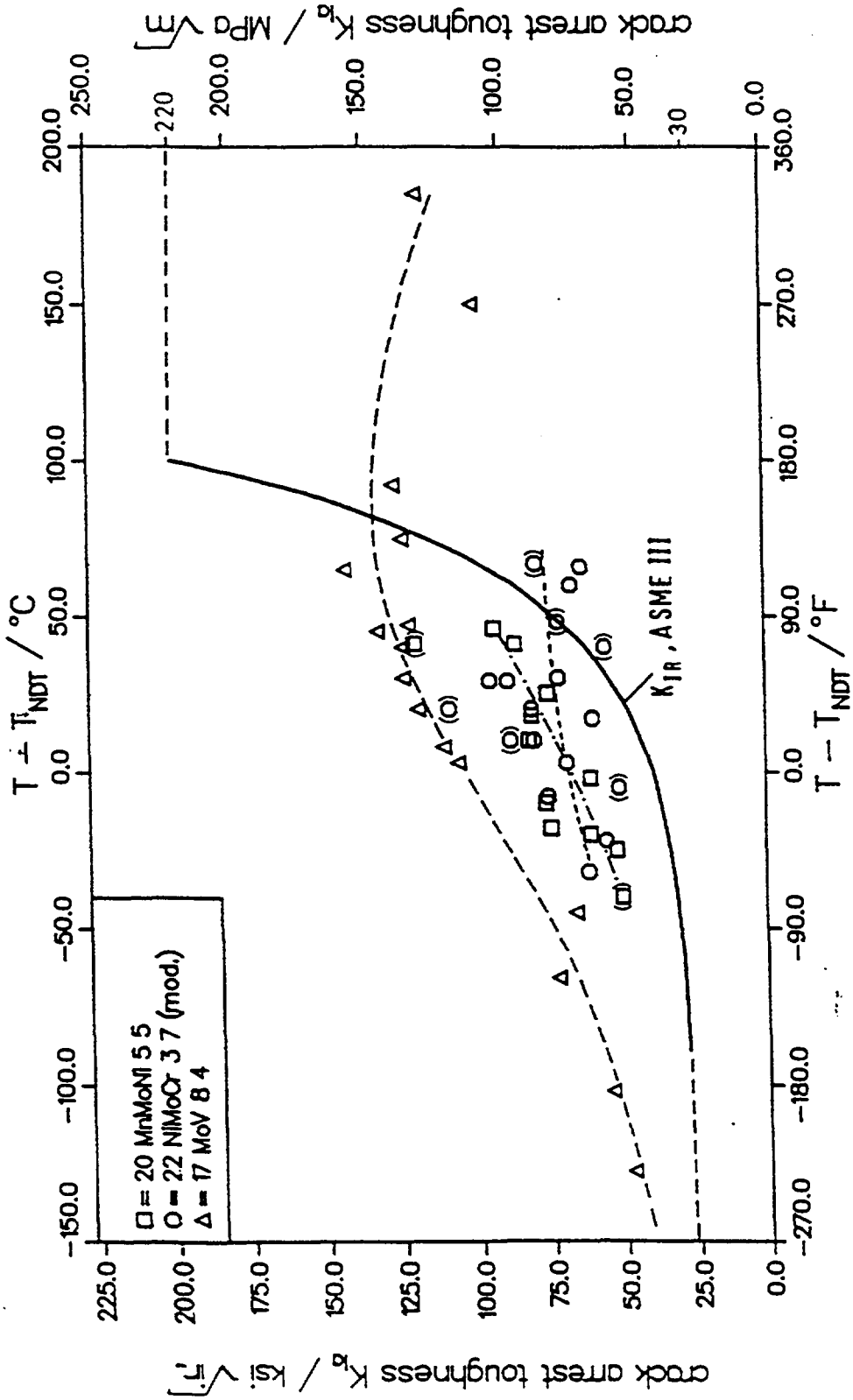
crack arrest toughness K_a / ksi $\sqrt{in.}$
crack arrest toughness K_a / MPa $\sqrt{m}$
T + T_{NDT} / °C
T − T_{NDT} / °F
□ = 20 MnMoNi 5 5
○ = 22 NiMoCr 3 7 (mod.)
△ = 17 MoV 8 4
K_{IR}, ASME III

FIGURE 26

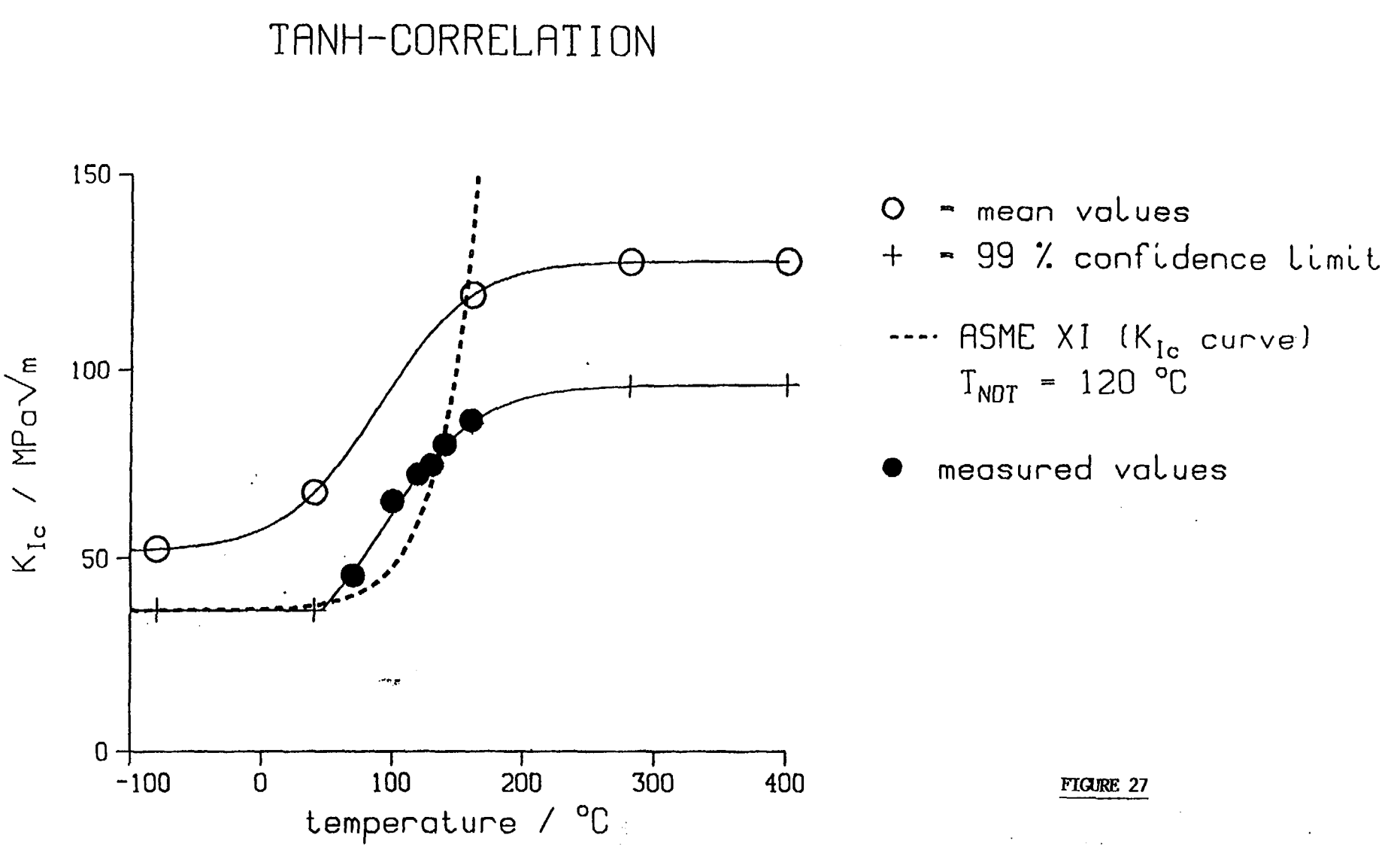
TANH-CORRELATION
150
100
50
0
K_{Ic} / MPa$\sqrt{m}$
-100
0
100
200
300
400
temperature / °C
○ = mean values
+ = 99 % confidence limit
---- ASME XI (K_{Ic} curve)
T_{NDT} = 120 °C
● measured values

FIGURE 27

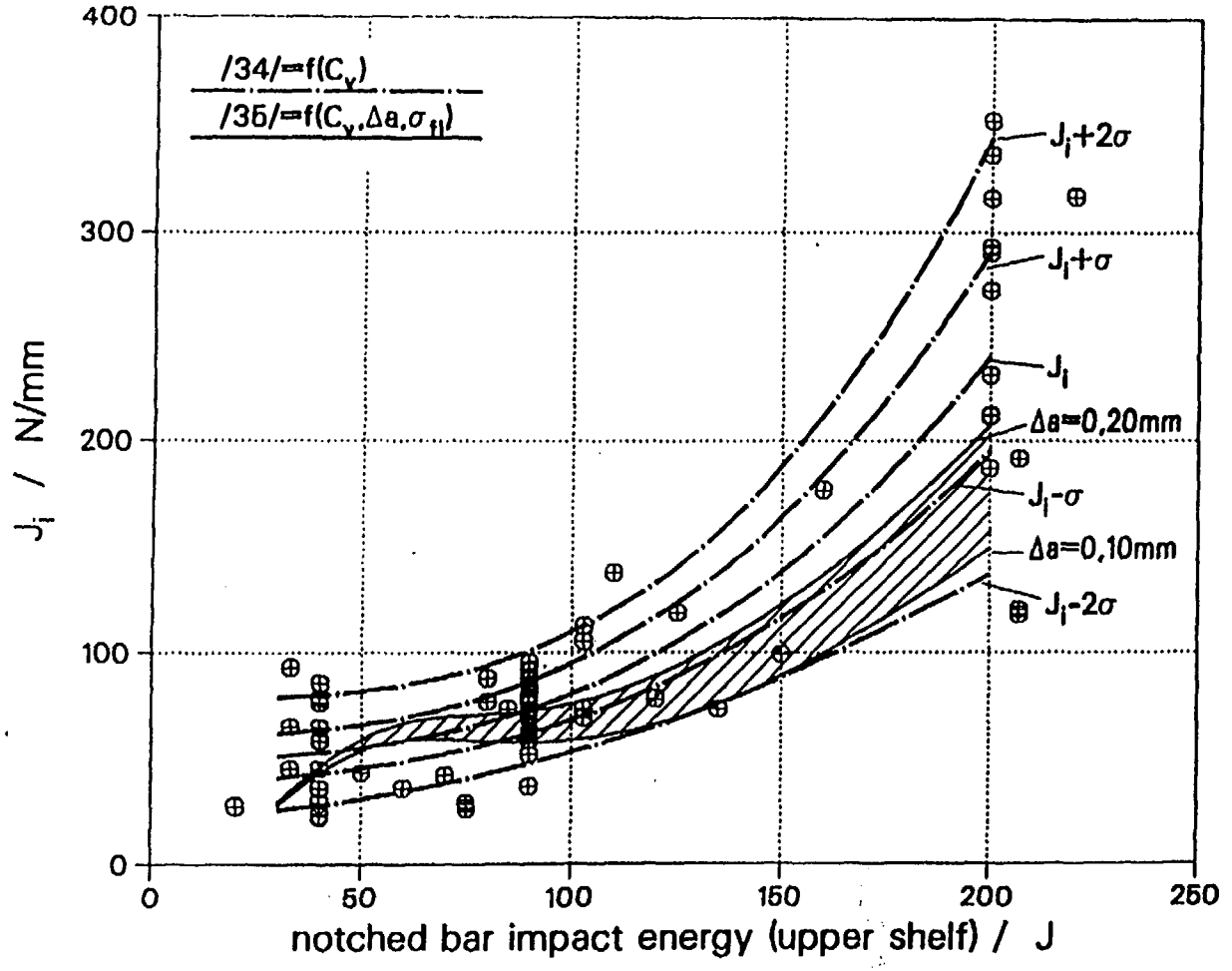
/34/=f(C_V)
/35/=f(C_V,Δa,σ_fl)
J_i+2σ
J_i+σ
J_i
Δa=0,20mm
J_i-σ
Δa=0,10mm
J_i-2σ
J_i / N/mm
notched bar impact energy (upper shelf) / J
0
100
200
300
400
0
50
100
150
200
250

FIGURE 28